NAVAL POSTGRADUATE SCHOOL

MONTEREY, CALIFORNIA

THESIS

GaAs/InAs MULTI QUANTUM WELL SOLAR CELL

by

Evangelos Koletsios

December 2012

Thesis Co-Advisors: Sherif Michael
                                        Gamani Karunasiri

Approved for public release; distribution is unlimited

THIS PAGE INTENTIONALLY LEFT BLANK

REPORT DOCUMENTATION PAGE		*Form Approved OMB No. 0704–0188*
Public reporting burden for this collection of information is estimated to average 1 hour per response, including the time for reviewing instruction, searching existing data sources, gathering and maintaining the data needed, and completing and reviewing the collection of information. Send comments regarding this burden estimate or any other aspect of this collection of information, including suggestions for reducing this burden, to Washington headquarters Services, Directorate for Information Operations and Reports, 1215 Jefferson Davis Highway, Suite 1204, Arlington, VA 22202–4302, and to the Office of Management and Budget, Paperwork Reduction Project (0704–0188) Washington DC 20503.		
1. AGENCY USE ONLY *(Leave blank)*	**2. REPORT DATE** December 2012	**3. REPORT TYPE AND DATES COVERED** Master's Thesis
4. TITLE AND SUBTITLE GaAs/InAs MULTI QUANTUM WELL SOLAR CELL		**5. FUNDING NUMBERS**
6. AUTHOR(S) Evangelos Koletsios		
7. PERFORMING ORGANIZATION NAME(S) AND ADDRESS(ES) Naval Postgraduate School Monterey, CA 93943–5000		**8. PERFORMING ORGANIZATION REPORT NUMBER**
9. SPONSORING /MONITORING AGENCY NAME(S) AND ADDRESS(ES) N/A		**10. SPONSORING/MONITORING AGENCY REPORT NUMBER**
11. SUPPLEMENTARY NOTES The views expressed in this thesis are those of the author and do not reflect the official policy or position of the Department of Defense or the U.S. Government. IRB Protocol number _____N/A_____.		
12a. DISTRIBUTION / AVAILABILITY STATEMENT Approved for public release; distribution is unlimited		**12b. DISTRIBUTION CODE** A
13. ABSTRACT (maximum 200 words)		

In this thesis, Silvaco software is used to form a precise, well-controlled reliable, and inexpensive solar-cell structure using quantum wells. Successful results will allow the exploitation of most of the advantages of quantum-well systems. This challenging research represents the first time that Silvaco simulation software has been used in the design of such a solar cell. This research field is promising because of the potential to increase the attainable energy efficiency of solar photon conversion, due to tunable bandgaps, which can absorb most of the solar spectrum, which conventional single-layer crystalline solar cells cannot do. The ultimate goal is the assembly of a quantum-well layer. A theoretical infinite-layer cell can reach an efficiency of 86% (constrained by thermodynamical limits). Quantum wells can reach 65%+ when a multilayer cell has reached 49%, and it is very expensive to build.

14. SUBJECT TERMS Solar cell, quantum wells, simulation, model, development, Silvaco, Atlas, InAs, GaAs			**15. NUMBER OF PAGES** 109
			16. PRICE CODE
17. SECURITY CLASSIFICATION OF REPORT Unclassified	**18. SECURITY CLASSIFICATION OF THIS PAGE** Unclassified	**19. SECURITY CLASSIFICATION OF ABSTRACT** Unclassified	**20. LIMITATION OF ABSTRACT** UU

NSN 7540–01–280–5500

Standard Form 298 (Rev. 8–98)
Prescribed by ANSI Std. Z39.18

i

THIS PAGE INTENTIONALLY LEFT BLANK

GaAs/InAs MULTI QUANTUM WELL SOLAR CELL

Evangelos Koletsios
Lieutenant, Hellenic Navy
B.S., Hellenic Naval Academy, 2001

Submitted in partial fulfillment of the
requirements for the degree of

MASTER OF SCIENCE IN APPLIED PHYSICS

from the

**NAVAL POSTGRADUATE SCHOOL
December 2012**

Author: Evangelos Koletsios

Approved by: Sherif Michael
                     Thesis Co-Advisor

                     Gamani Karunasiri
                     Thesis Co-Advisor

                     Andres Larraza
                     Chair, Department of Physics

THIS PAGE INTENTIONALLY LEFT BLANK

ABSTRACT

In this thesis, Silvaco software is used to form a precise, well-controlled reliable, and inexpensive solar-cell structure using quantum wells. Successful results will allow the exploitation of most of the advantages of quantum-well systems. This challenging research represents the first time that Silvaco simulation software has been used in the design of such a solar cell. This research field is promising because of the potential to increase the attainable energy efficiency of solar photon conversion, due to tunable bandgaps, which can absorb most of the solar spectrum, which conventional single-layer crystalline solar cells cannot do. The ultimate goal is the assembly of a quantum-well layer. A theoretical infinite-layer cell can reach an efficiency of 86% (constrained by thermodynamical limits). Quantum wells can reach 65%+ when a multilayer cell has reached 49%, and it is very expensive to build.

THIS PAGE INTENTIONALLY LEFT BLANK

TABLE OF CONTENTS

LIST OF FIGURES

LIST OF TABLES

THIS PAGE INTENTIONALLY LEFT BLANK

EXECUTIVE SUMMARY

Several theses have been written on generating electrical power from renewable sources of energy. These sources are free and abundant in nature and render structures using them energy independent. Most of the existing theses have explored solar power, which suggests that solar power is seen as the best solution. The Naval Postgraduate School is fortunate to have a very important tool for research, Silvaco Atlas, which uses a virtual wafer-fabrication suite of tools. This simulation software gives the ability to "build"—meaning simulate—solar cells without the cost of the exotic materials needed to build a real solar cell.

Designing solar cells on computers is somewhat new. Panayiotis Michalopoulos made the first effort with brilliant work in designing a solar cell using Silvaco in March 2002. He designed a prototype triple-multijunction solar cell with 29.5% efficiency. Several follow-up attempts were made, the last and most important by Michael Hideto Tsutagawa in his December 2012 thesis "Triple Junction InGaP/GaAs/Ge solar cell optimization using Silvaco Atlas," which has been characterized as critical technology because he achieved an efficiency of 36.283%.

This thesis uses part of the Silvaco Atlas codes that were optimized in previous research for achieving high efficiency. However, main thrust is to simulate the addition of a quantum-well region inside the existing solar cell design. The incorporation of quantum-well regions than conventional multilayers may lead to the achievement of theoretically predicted 85% efficiency.

Quantum-well technology may be new as an idea, but it is still part of semiconductor physics, as multijunction cells are. Although solar cells have always been considered the spearhead of the innovation in semiconductors, for reasons unclear they have nowadays been left behind. Hopefully, through this thesis there will be a reboot in the development of solar cells, using state-of-the-

art technology, incorporating nanostructures. The results of this effort can be judged as success only if experimental data verify simulation results.

ACKNOWLEDGMENTS

THIS PAGE INTENTIONALLY LEFT BLANK

I. INTRODUCTION

A. BACKGROUND

Using Silvaco for virtualizing solar cells can be considered a new area of research. It was in 2002 that P. Michalopoulos [1] made the first, successful step in this area, and others have followed with substantive research too. But designing solar cells with quantum dots/wells is a totally new area, with no record of previous tries. There have been several fabrications of quantum wells/dots by epitaxial growth, or by preparing each quantum dot separately, or by preparing a quantum well and depositing layer upon layer—and many other alternatives. There also have been several choices concerning the combination of materials. Although the area is very promising, nothing has yet been found that seems able to replace the triple-junction solar cell. From what has been tested so far, the possibility that gives highest expectations is InAs/GaAs quantum dots/wells.

B. OBJECTIVE

The objective of this thesis is not only to design InAs/GaAs quantum wells, but to combine them with a multijunction solar cell. This will substitute expensive solar cells with cheaper ones without sacrificing efficiency—and in the future maybe yield higher efficiency—and make solar power the replacement for fossil fuel. Silvaco Atlas will virtualize the whole research. Already-successful codes will be used, and by depositing quantum-well layers, an attempt to boost efficiency will be made. Until now, there has been no code in Silvaco that builds quantum-well layers, and Silvaco Atlas manuals [2] provide no specific information for this area of research. The effort will be made to build manually these layers and virtualize quantum wafers. Furthermore, optimizations will be tried in known structures, involving thickness of layers, materials, and doping.

1

C. RELATED WORK

The Naval Postgraduate School has many thesis concerning multijunction solar cells, but none concerning quantum-well solar cells. This research should be considered novel.

D. ORGANIZATION

In this thesis, chapters are organized so that a reader with no knowledge in this area will be able to get the basic concepts in physics and a general picture of a solar cell. Therefore, Chapter II is an introduction to semiconductors, Chapter III talks about quantum theory and nanostructures, Chapter IV combines chapters II and III with general principles of solar cells to build a quantum well solar cell, and in Chapter V the result of previous chapters is designed in Silvaco Atlas. Chapter VI draws conclusions about the whole research and makes recommendations for future research.

II. SEMICONDUCTORS

A. INTRODUCTION

A great burst in technology has occurred in the last few years in the development, optimization, and extended use of semiconductors. Semiconductors have the ability to function either as an insulator or a conductor, depending on the needs of the manufacturer. The properties of these materials are remarkable because of their tunable characteristic, which is conductivity. Conductivity depends on temperature—a factor that we cannot fully control—and on the energy bandgap. The energy bandgap is the energy difference between the two energy bands, that is, conduction and valence band.
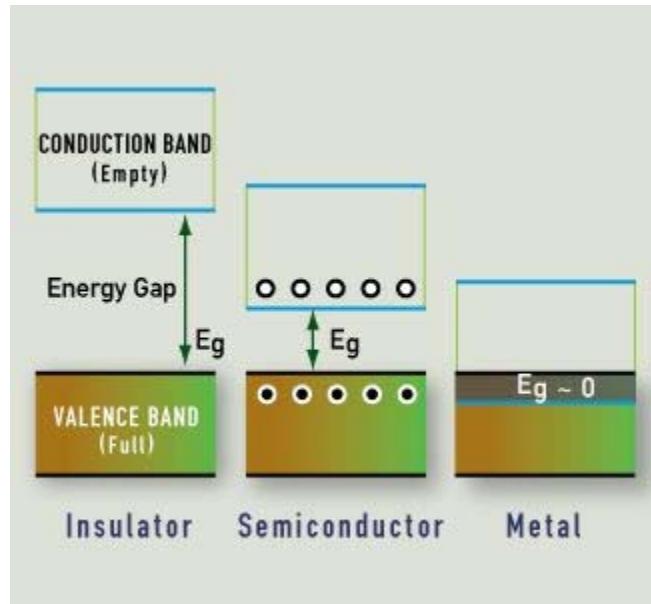
Figure 1.   Energy-Band Gap for Insulator, Semiconductor and Metal [from Ref. 2]

This is a forbidden energy region for electrons. Therefore, for conductivity, electrons should be able to overcome this region. External energy might be

electrical power, which would result in light production, but it can also absorb light to produce electrical energy. That is why solar cells were created.
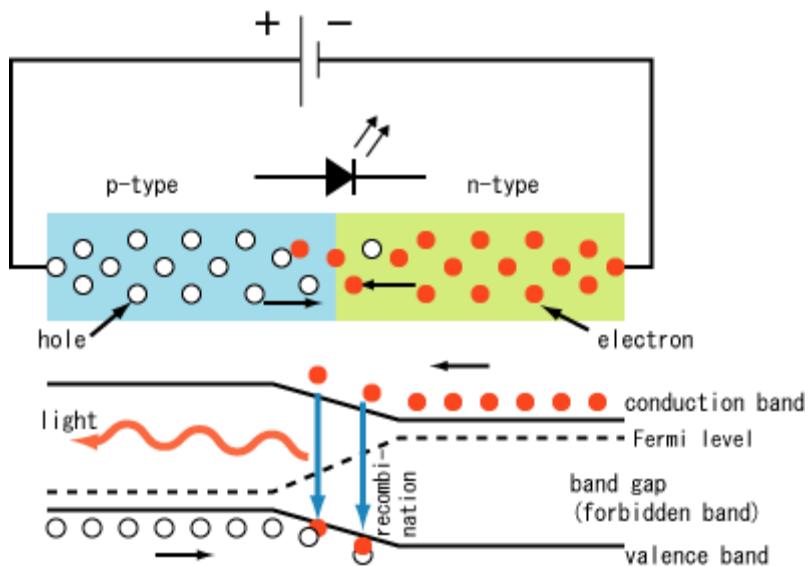
Figure 2. Light-Emitting Diode (LED) [from Ref. 2]
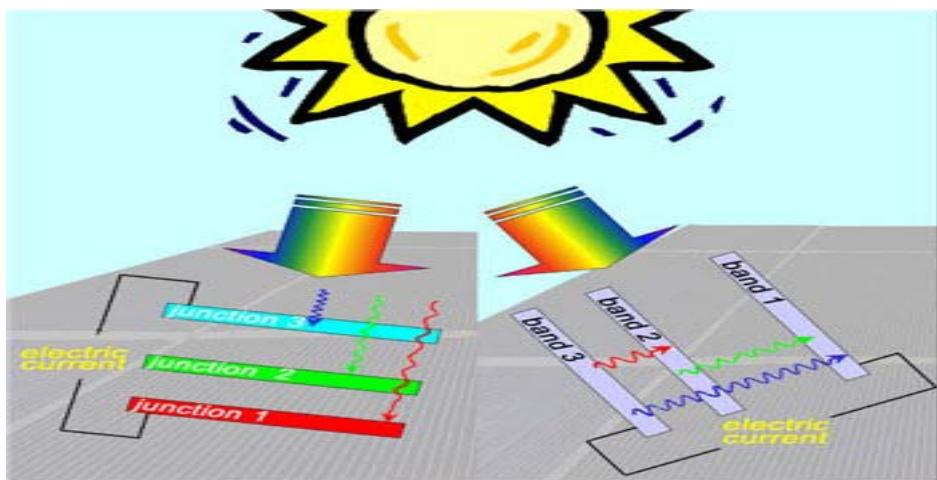
Figure 3. Solar Cell [from Ref. 2]

As temperature increases, electrons excited can occupy the conduction band enter excited states, which explains the temperature dependence of these materials and the thermoelectric or Seebeck effect.
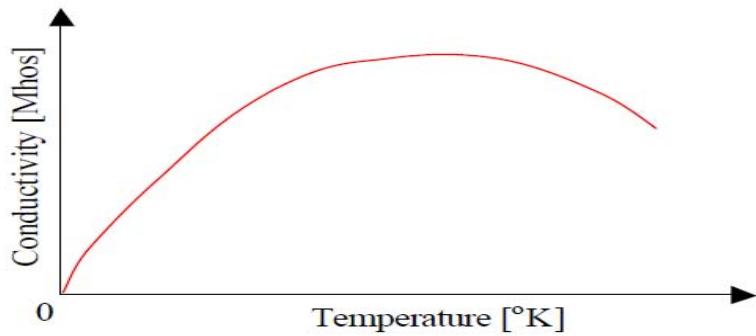
Figure 4.   Temperature dependence of conductivity [from Ref. 1]

The thermoelectric field E is given by the equation:

$$E = Q \frac{dT}{dx} \tag{1}$$

where Q=thermoelectric power and describes n- or p- type domination.

In n-type semiconductors, electrons are the majority and are close to the conduction band. The presence of these extra electrons creates additional energy levels below the conduction band, called donors levels. When they are leaving the valence band and go to the conduction band, thereby producing electric current, they leave vacancies, which are called holes. For experimental reasons, holes are considered positive charges. The semiconductors that contain a majority of holes or positive charges are called p-type semiconductors. The presence of these extra holes creates additional energy levels above the valence band, called acceptor levels [2].
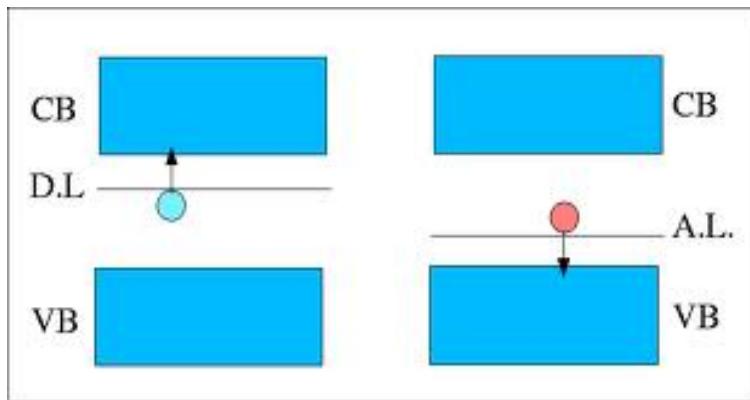
Figure 5.   Energy band of semiconductors [from Ref. 2]

A semiconductor that contains an equal number of electrons and holes is called intrinsic; otherwise, it is extrinsic.

B.   INTRINSIC SEMICONDUCTORS

In nature, there are no intrinsic materials. In fact, it is very difficult even to produce them, but it is easier to study their properties and calculate characteristics such as current density J, drift mobility, conductivity and others.

1.   Electrons and Holes

In the previous chapter, we saw that for an electron to leave the valence band (due to excitation) and reach the conduction band, it needs energy. This energy must be larger than the energy gap,

$$E > E_g \tag{2}$$

and it is calculated by the equation

$$E = hv \tag{3}$$

where h is Planck's constant and v is the frequency of the photon. The result of this excitation is a free electron in the conduction band, which, with the presence of an electrical field, will create a hole in the valence band, which travels around the crystal as a positive charge and lattice vibration. If this electron is not

6

collected, then, due to preservation of energy, the opposite procedure will happen. The electron will return to the valence band to fill the hole and a photon will be emitted. This phenomenon is called recombination.

If we apply an electrical field, two things happen. Energy bands will be bent and free electrons and holes will both result in the conductivity of the semiconductors, as it is shown in Figure 6.
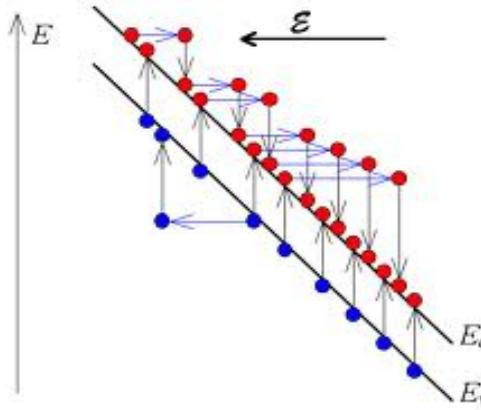
Figure 6.   Electrical Field [from Ref. 3]

The current density that is created is given by the equation,

$$J = enu_e + epu_h \tag{4}$$

$$u_{e/h} = \mu_{e/h} E_x \tag{5}$$

Where u_e and u_h are the drift velocities, n and p are the concentration, and μ_e and μ_h drift mobilities of electrons and holes, respectively [3]. From the above equations, the semiconductor conductivity is

$$\sigma = en\mu_e + ep\mu_h \tag{6}$$

2. Fermi Energy

The energy of the last-occupied level of a system of fermions at absolute zero is called Fermi energy E_F. Typical values of the Fermi energy are ~ 5 eV, given by equation (7):

$$E_F = \frac{\hbar^2}{2m}(3\pi^2 n)^{2/3} \qquad (7)$$

where n is the number of electrons per unit volume.

The energy density of states g(E) serves to reveal if there is uniform distribution of the number of electrons in different energy states. Defined as the number of energy states per unit volume, corresponding to energy E in the energy range around the value of dE, how many states exist per unit volume with energy between E + dE.
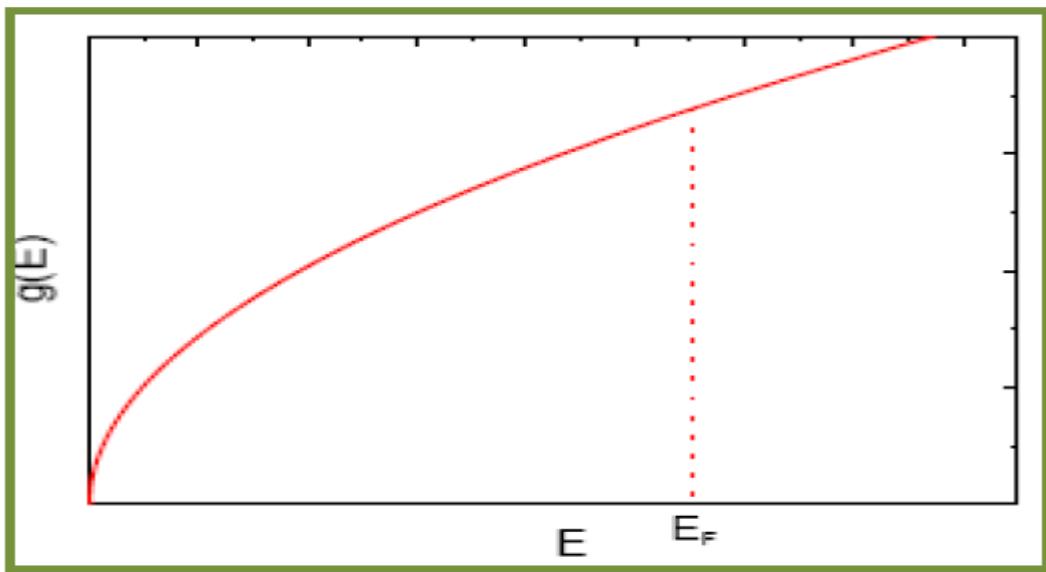
Figure 7.   Density Chart vs Energy [from Ref. 1]

From Figure (7), the density of energy states increases with E. This means that most situations are available for free electrons at higher energies. The density of states per unit volume is given by equation (8):

$$N(E) = g(E)/V(E) \tag{8}$$

where V is the volume of the solid.

3.   Electron and Hole Concentrations

To calculate electron (n) and hole (p) concentrations, we must first introduce the density and effective density of states.

The density of states is the number of states per unit energy, per unit volume [4], and with the Fermi–Dirac function, we determine concentration.

$$n_E d_E = g_{cb}(E) f(E) dE \tag{9}$$

The effective density of states is a constant, N, which is temperature dependent and which we introduce for conduction and valence band.

$$N_{c/u} = 2(\frac{2\pi m_{e/h}^* kT}{h^2})^{3/2} \tag{10}$$

$$n = N_c \exp\left[-\frac{(E_c - E_f)}{kT}\right] \tag{11}$$

$$p = N_u \exp\left[-\frac{(E_f - E_u)}{kT}\right] \tag{12}$$

$$np = N_c N_u \exp\left[-\frac{E_g}{kT}\right] \tag{13}$$

In this case, involving intrinsic semiconductors, hole and electron concentrations are equals

$$n = p = n_i \tag{14}$$

Therefore, equation (13) at thermal equilibrium becomes

$$n_i^2 = N_c N_u \exp\left[-\frac{E_g}{kT}\right] \tag{15}$$

which corresponds to mass-action law. Another importance of mass-action law is that the product of *n*p* is proportional to recombination and rate of generation.

C. EXTRINSIC SEMICONDUCTORS

As mentioned in the previous paragraph, in nature it is extremely difficult to find intrinsic semiconductors, due to impurities. The impurities characterize a material as extrinsic and, depending on their nature, affect hole and electron concentration.

1. Doping *p* and *n* Type

The materials that can be mixed and create bonds can be found if we look on the periodic table at their valency.
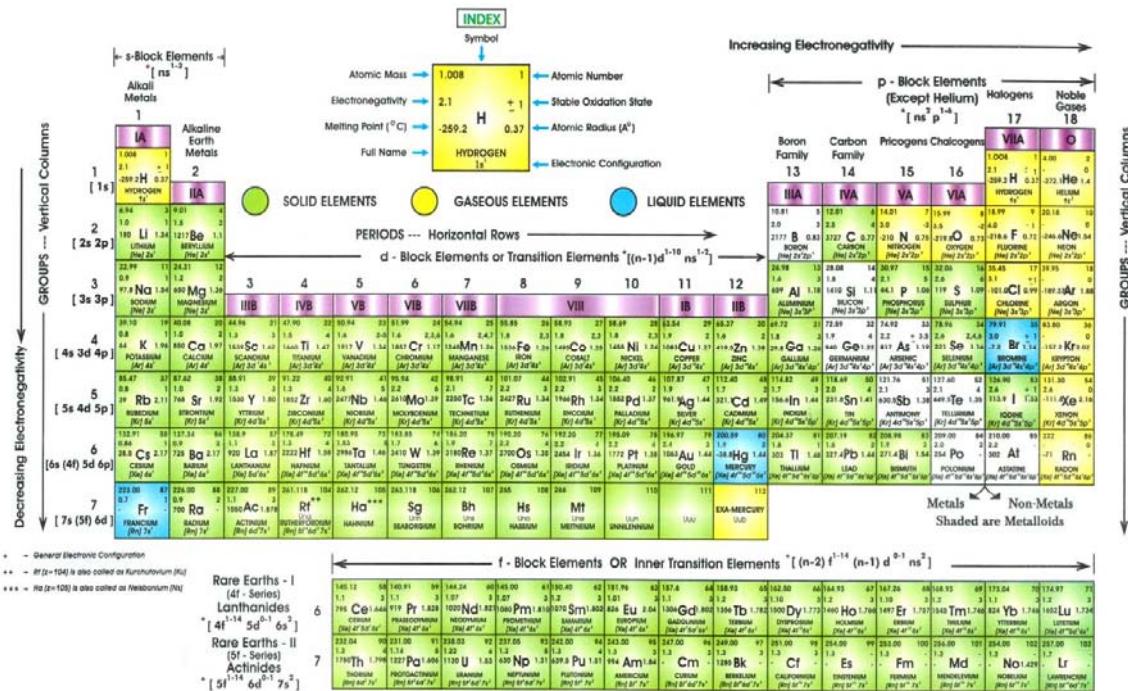
Table 1.   Periodic Table [from Ref. 1]

In *n*-type doping, we add at the intrinsic semiconductor e.g., that belongs at group IV, atom-donors, with five valence electrons. This means that the extra electron will be free in the new bond and will increase the material's conductivity significantly.

In *p*-type doping, we add atom-acceptors, with three valence electrons. This will result in the creation of one hole, which will be ready to accept an electron.

In both cases the materials remain neutral.

Except for *p* or *n* doping, the situation also arises where the material is both *p* and *n* doped. This is called compensation doping, and happens at room temperature. This doesn't change the general rule $np = n_i^2$ with the difference that when we have more donors

$$n = N_d - N_a \tag{16}$$

and when we have more acceptors

$$p = N_a - N_d \tag{17}$$

2. Temperature Dependence

As with intrinsic semiconductors, so with extrinsic: temperature affects concentration. The equation that describes this dependence is slightly different from that of intrinsic:

$$n = \left(\frac{1}{2}N_c N_d\right)^{1/2} \exp\left(\frac{-\Delta E}{2kT}\right) \tag{18}$$

This expression is for low temperature and shows that when temperature is increasing, donors give their electrons to the conduction band because of their ionization. At one point, all donors are ionized, so the concentration of the electrons is equal with the concentration donors $n=N_d$. At very high temperatures, the material behaves as intrinsic.

We can separate the temperature dependence into three regions: low ($T<T_s$), medium ($T_s<T<T_i$), and high ($T>T_i$) temperature range, where T_s is saturation temperature.
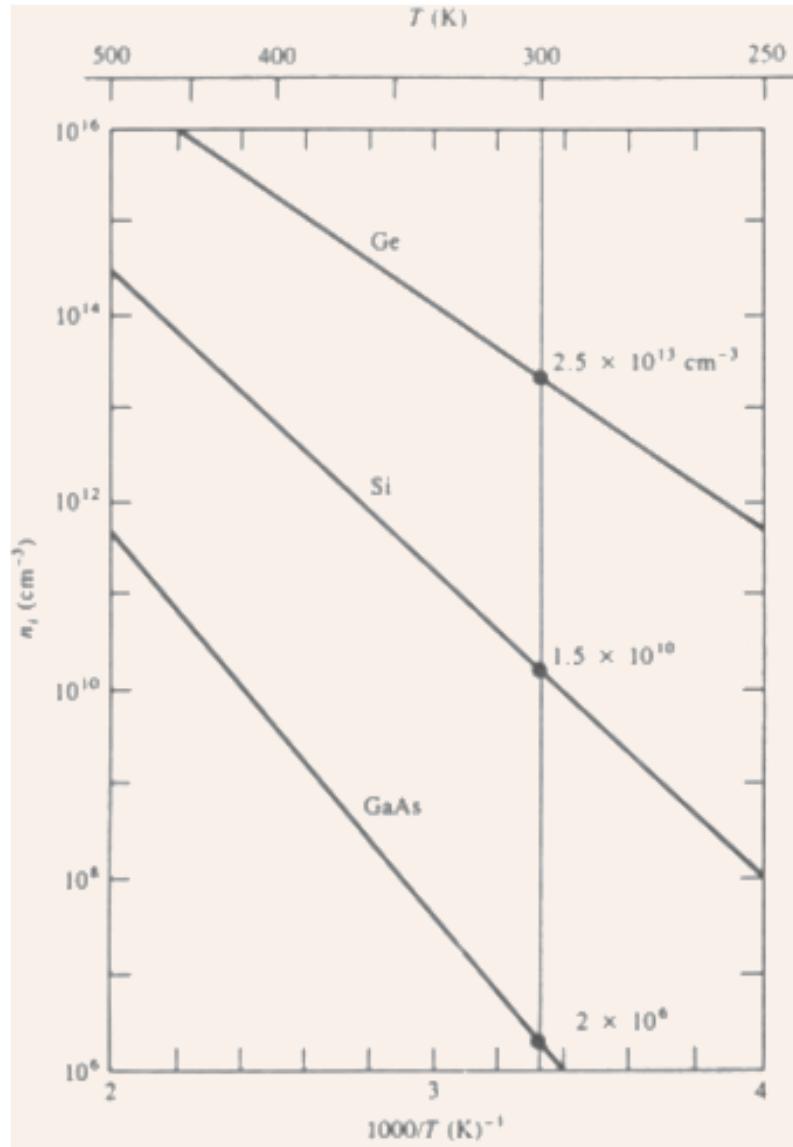
Figure 8.   Temperature dependence of intrinsic concentration [from Ref. 7]
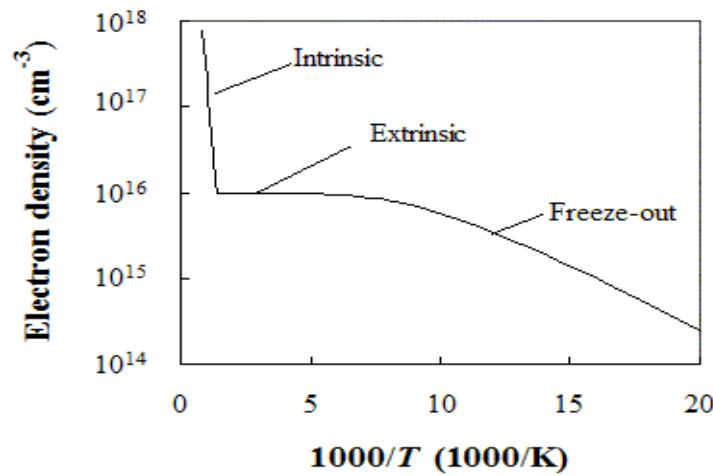
Figure 9.   Temperature dependence of extrinsic concentration [from Ref. 7]

Another area that change of temperature affects is mobility. Mobility, or rate scattering, decreases as temperature rises, and can be better described in Figure 9.
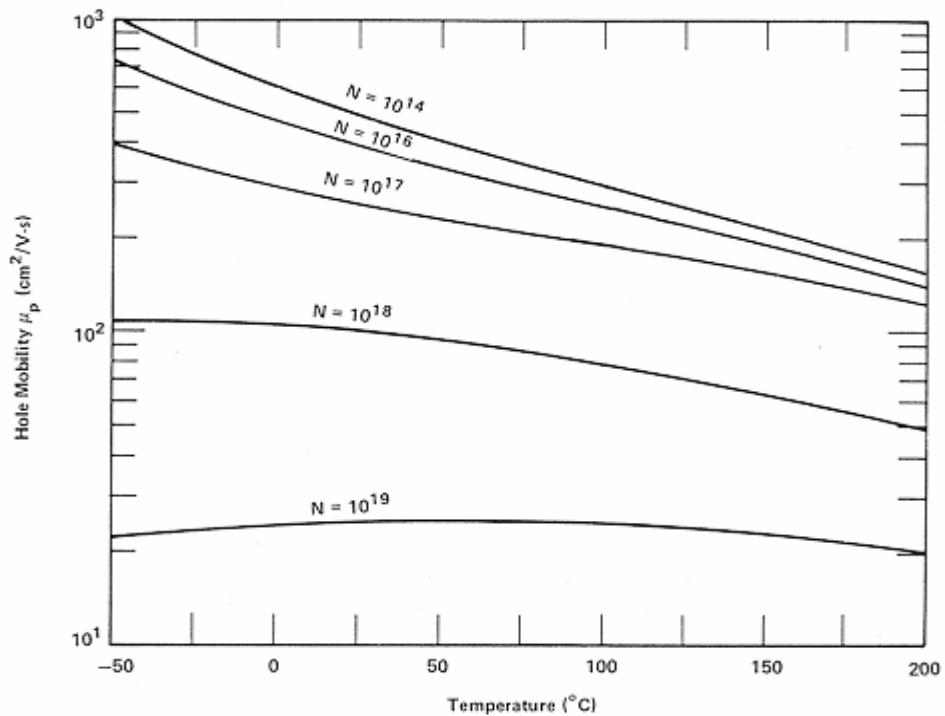
Figure 10.   Temperature dependence of electron drift mobility [from Ref. 7]

13

Finally, and most important, conductivity behaves similar to concentration as temperature increases. The reason is that it depends directly on temperature, as can be seen from conductivity equation, which is proportional to equation (18).

$$\sigma = en(\mu_e + \mu_h) \tag{19}$$

D. RECOMBINATION

Recombination is the process by which a free electron on the conduction band runs into a hole and falls into a low-energy, empty electronic state [3]. This results in energy transitioning to photon energy $E_g=h\nu$, which is used in many applications like light-emitting diodes (LEDs) and lasers. However, this equation is not always correct. It depends on how the conduction and valence bands are aligned, and we meet two possibilities, direct and Indirect. In a direct bandgap, an electron can directly emit a photon so the above equation is correct, because the momentum of the electrons in the conduction band is the same as the momentum of the holes in the valence band. In an indirect bandgap, where the momentums are not the same, the equation is incorrect, but the basic principles of conservation of momentum and energy are satisfied

$$\hbar\vec{k}_f = \hbar\vec{k}_i + \hbar\vec{k}_{photon} + \hbar\vec{k}_{phonon} \tag{20}$$

$$E_f = h\nu - E_i \pm E_p \tag{21}$$

Quantum mechanics helps as understand belter the way en electron behaves. If an electron is in a potential well, then its energy is given by the equation

$$E_n = \frac{(\hbar k_n)^2}{2m_e} \tag{22}$$

It is quantized, where $k_n = \dfrac{n\pi}{L}$ and *L* the size of the potential well. The electrons's average potential energy inside the crystal is considered to be zero, and outside,

large. To be able to find the energy according to its location inside the crystal, we use the Schrödinger equation

$$\frac{\partial^2 \psi}{\partial x^2} + \frac{2m_e}{\hbar^2}[E - V(x)]\psi = 0 \qquad (23)$$

Solving equation (23) we find the electron Bloch-wave function.

$$\psi_k(x) = U_k(x)\exp(jkx) \qquad (24)$$

Where $U_k(x)$ is a potential-energy-dependent periodic function and *hk* is the momentum in the photon-absorption process, or crystal momentum. At temperatures above zero, some electrons will be excited from the valence to the conduction band because of thermal excitation. After recombination, the electron will return to the valence band without any change in k value, which complies with momentum conservation, considering also that the emitted photon momentum is negligible to electron momentum. But this is for a one-dimensional crystal and three-dimensional crystals that are similar, such as a GaAs crystal, which is mainly used in solar cells and it is described as a direct bandgap semiconductor. On the other hand, for crystals like Si, direct recombination does not happen, but indirect. To comply with conservation of momentum, indirect recombination consists of a third body and a center of recombination and is described by equations (20) and (21).

It is important to mention an unwanted phenomenon in this procedure called charge-carrier trapping, which limits device performance. In this phenomenon, an electron can be trapped and lost in a localized state that is not in the conduction band. This happens due to crystal imperfections.
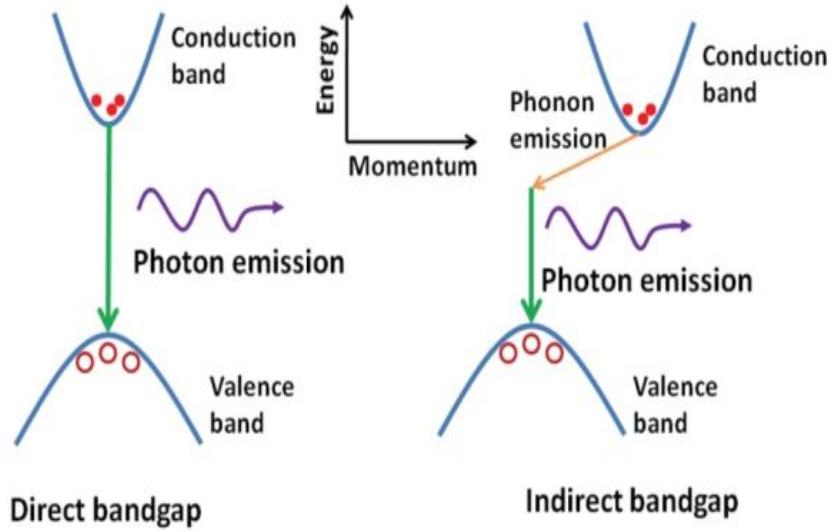
Figure 11.   Direct and Indirect Bandgap [from Ref. 8]

E.   ABSORPTION

Light absorption depends completely on bandgap; therefore bandgap energy E_g is the most important factor in solar cells. If the photon energy is smaller than the bandgap energy, there will be no absorption. If it is much larger, the extra energy $hv\text{-}E_g$ will be lost into lattice vibrations. To study absorption, we use *absorption coefficient (α* to study the optical parameters of semiconductors. Indirect bandgap is proportional to equation (22), and indirect to equation (23).

$$a(hv) \propto \left(hv - E_g \right)^{1/2} \tag{25}$$

$$a(hv) \propto \left(hv - E_g \pm E_p \right)^{2} \tag{26}$$

Generally absorption coefficient is defined by

$$a = -\frac{\delta I}{I \delta x} \tag{27}$$

and by integrating leads to Beer–Lambert law, where I is the light intensity and I_o the energy incident per unit area per unit time [4].

16

$$I = I_o \exp(-ax) \tag{28}$$
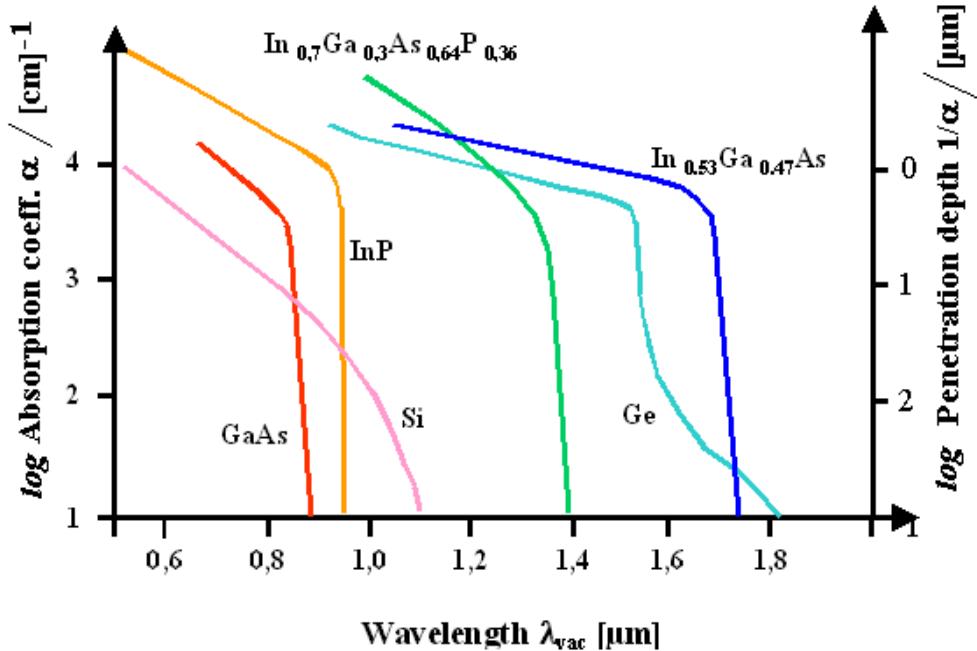
Figure 12.   Absorption coefficient [from Ref. 4]

Absorption increases when the available states in the conduction and valence bands increase, which is reasonable from the time that electrons must find empty spaces in order to be excited. If photon energies are high enough, electrons can even be excited from the valence band to a vacuum.
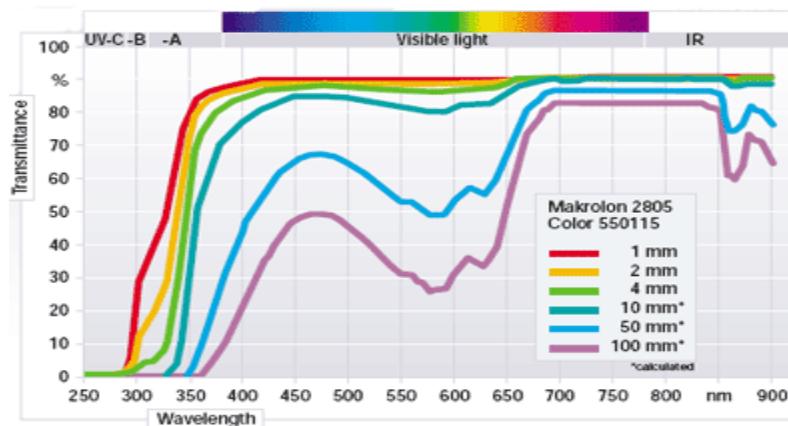
Figure 13.   Transmittance as a function of wavelength (250–900 nm)

F. CRYSTAL STRUCTURE

To build a solar cell is not as easy as it seems. If crystal structure did not matter, we would be able to choose materials with variable bandgaps, put them in the right order and take advantage of the total spectrum, achieving very high efficiencies. However, it does matter. The atom model differs from material to material and is best described by the Bohr model. Table 1 gives the basic information of an atom; we can see which atom bonds with what or which metal we can dope with. A common crystal structure of a semiconductor is shown in Figure 14.
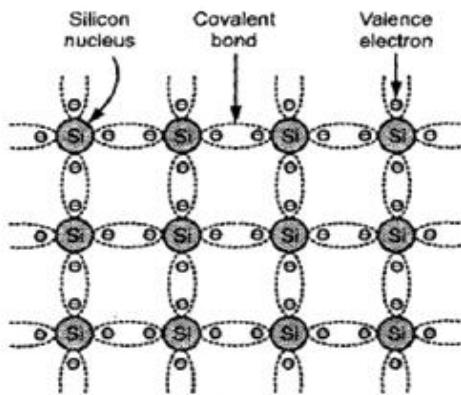
Figure 14. Structure of intrinsic semiconductor

A p- or n-doped semiconductor is shown in Figure 15.
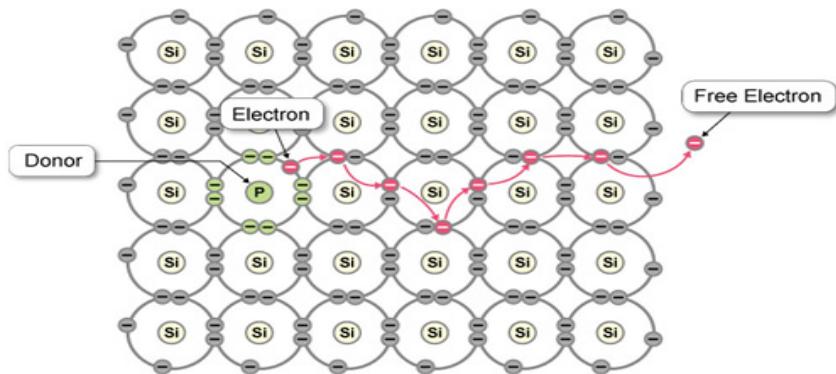
Figure 15. Structure of doped semiconductor

There are several types of bonding, such as covalent, metallic, ionic, secondary, and others. In the area of semiconductors, what interests us most is mixed bonding.

An example of mixed bonding is GaAs. Ga and As share electrons. This makes a covalent bond. Nevertheless, because they are two different atoms, their electrons are not equally shared, which gives some ionic character. This type of mixed bond is called a polar bond. The difference in electron-attracting ability is called electronegativity, and it is measured on the Pauling scale, which gives an electronegativity value of X. For two atoms A and $B,$ the difference X_A-X_B measures a bond's polar/ionic properties.

As mentioned above, not every atom can bond with another. A lattice match is needed. Such fabrication is very important in heterostructures where we want to combine materials with variable bandgaps. Figure 16, combining the energy bandgap and lattice constant, shows how can we build possible material systems and more specifically, how can we build a GaInP.
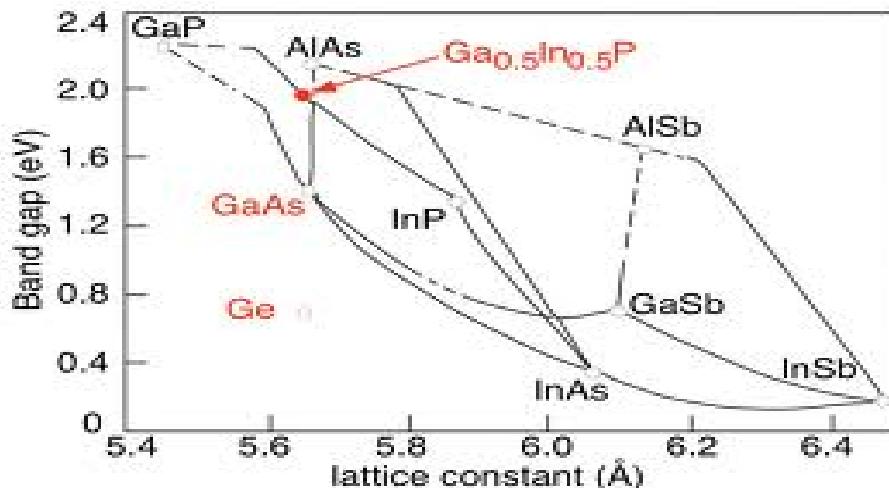
Figure 16.   Possible material systems [from Ref. 8]

To be able to build such combinations we need Vegard's law, which combines consistency with the lattice constant and extends to bandgap calculation. But it is not the same for all materials. For InPAs and AlGaAs,

19

$$a_{InPAs} = xa_{InP} + (1-x)a_{InAs} \tag{29}$$

$$Eg_{AlGaAs} = xEg_{AlAs} + (1-x)Eg_{GaAs} \tag{30}$$

But generally, we use Table 2.

Compound	Energy Gap
$Al_xIn_{1-x}P$	1.351+2.23x
$Al_xGa_{1-x}As$	1.424+1.247x
$Al_xIn_{1-x}As$	$0.360+2.012x+0.698x^2$
$Al_xGa_{1-x}Sb$	$0.726+1.129x+0.368x^2$
$Al_xIn_{1-x}Sb$	$0.172+1.621x+0.43x^2$
$Ga_xIn_{1-x}P$	$1.351+0.643x+0.786x^2$
$Ga_xIn_{1-x}As$	0.36+1.064x
$Ga_xIn_{1-x}Sb$	$0.172+0.139x+0.415x^2$
GaP_xAs_{1-x}	$1.424+1.150x+0.176x^2$
$GaAs_xSb_{1-x}$	$0.726–0.502x+1.2x^2$
InP_xAs_{1-x}	$0.360+0.831x+0.101x^2$
$InAs_xSb_{1-x}$	$0.18–0.41x+0.58x^2$

Table 2.   Possible Material Systems [from Ref. 8]

For $Ga_xIn_{1-x}P$ from Figure 16, we see we can combine GaP and InAS to create this semiconductor, which can be a III-V direct or indirect bandgap, and with the above equations and table, we can define the material's concentration, *x=0.5.* Thus we come to our final product, $Ga_{0.5}In_{0.5}As$.

G.   JUNCTIONS

A photovoltaic cell is a basic a pn-junction diode where p-type and n-type semiconductors are combined, as shown in Figure 17.
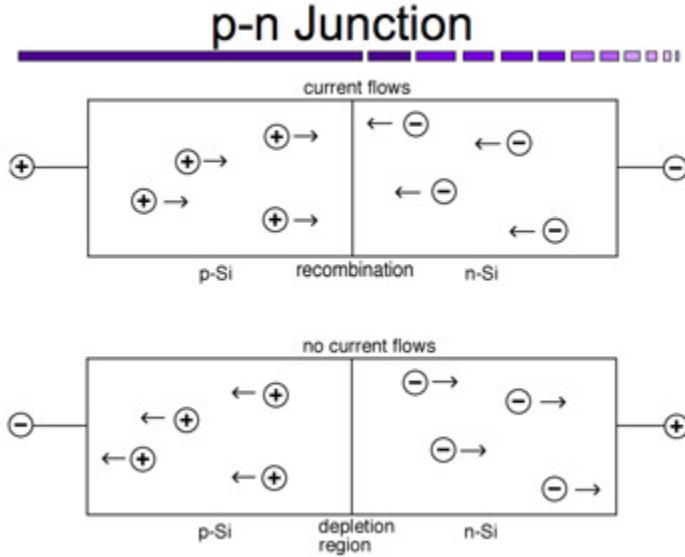
Figure 17.　P-N Junction [from Ref. 2]

In this junction, current flows easily in one direction, but almost none flows at the other, under external bias.

Two currents exist in this diode: thermal-electron current, which is created by thermal excitation of the electrons, and recombination current, which is created when free electrons from n-semiconductor drift to p-semiconductor. In the area where p- and n-semiconductors connect, a space-charge layer, or the depletion region, is created. Depending on how much each region is doped, the depletion region is moving towards the higher doped area. In this situation, there is no external voltage—thermal and recombination current are equal and cancel each other out. There is also a built-in voltage, which is related to doping concentration and material properties.

$$V_0 = \frac{kT}{e} \ln\left(\frac{N_a N_d}{n_i^2}\right) \tag{31}$$

Under external bias, we meet two situations: forward and reverse bias.

In forward bias, the positive pole is connected to p-semiconductor. Electrons due to an internal electric field are helped to move the direction they

intended to move in, resulting in a steady current flow. Not only electrons, but holes also diffuse towards the n-semiconductor. To study electron behavior at room temperature under forward bias, we use Maxwell–Boltzmann statistics. Therefore, we meet three currents, the diffusion, the recombination, and the total current:

$$I_D = I_{so}(e^{eV/kT} - 1) \tag{32}$$

$$I_R = I_{Ro}(e^{eV/2kT} - 1) \tag{33}$$

$$I_{Total} = I_0(e^{eV/kT} - 1) \tag{34}$$

In reverse bias, the positive pole of a bias is connected to the n-semiconductor. In this case, there is a small negative current. The negative pole attracts holes and the positive pole attracts electrons. But there are is no electron pumping, so electron movement cannot be sustained. Increasing the voltage has a limit, above which the pn junction breaks down and a large reverse current is created. This results in temperature increase, destroying the device by melting the contacts.

The approximation of the I–V curve is shown in Figure 18.
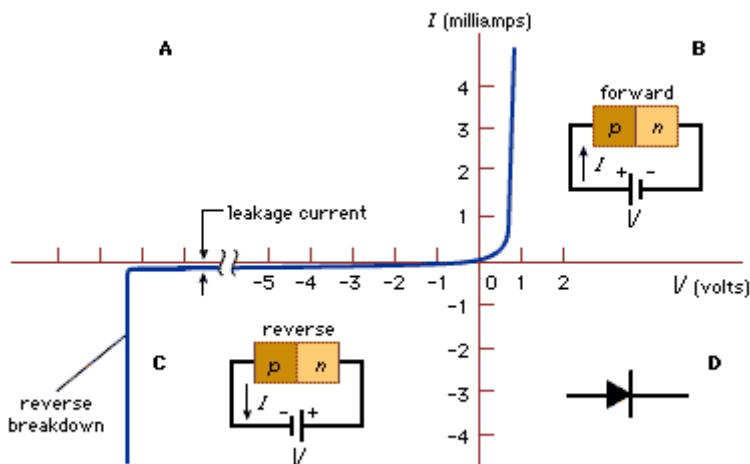
Figure 18.   I–V Curve for PN-Junction Diode

22

III. QUANTUM THEORY

A. INTRODUCTION

In the 1970s Esaki and Tsu made a discovery/invention that gave a new perspective in mechanics: semiconductor quantum wells. This led from classical mechanics to quantum.

The wavelength of a wave is given by the De Broglie equation (35)

$$\lambda = h\big/p \tag{35}$$

where *p* is the momentum and arises as an eigenvalue and leads to a kinetic energy eigenvalue

$$T = \frac{\hbar^2 k^2}{2m} \tag{36}$$

In a vacuum, the total energy is the kinetic energy, as described by the time-independent Schrödinger equation (37)

$$-\frac{\hbar^2}{2m}\nabla^2\psi = \mathrm{E}\,\psi \tag{37}$$

and time-dependent Schrödinger equation (38)

$$\iota\hbar\frac{\partial}{\partial t}\psi = \mathrm{E}\,\psi \tag{38}$$

To apply the Schrödinger equation to electrons, we introduce *effective mass m,*[*] and the general form of Schrödinger equation is

$$-\frac{\hbar^2}{2m^*}\frac{\partial^2}{\partial z^2}\psi + V\psi = \mathrm{E}\,\psi \tag{39}$$

B.   QUANTUM-WELL ENERGY GAP

In well structures, the energy gap is not the same as that of a bulk material. The reason for this phenomenon is that in z direction, quantization of energy occurs. The following figure shows the structure of a quantum well.
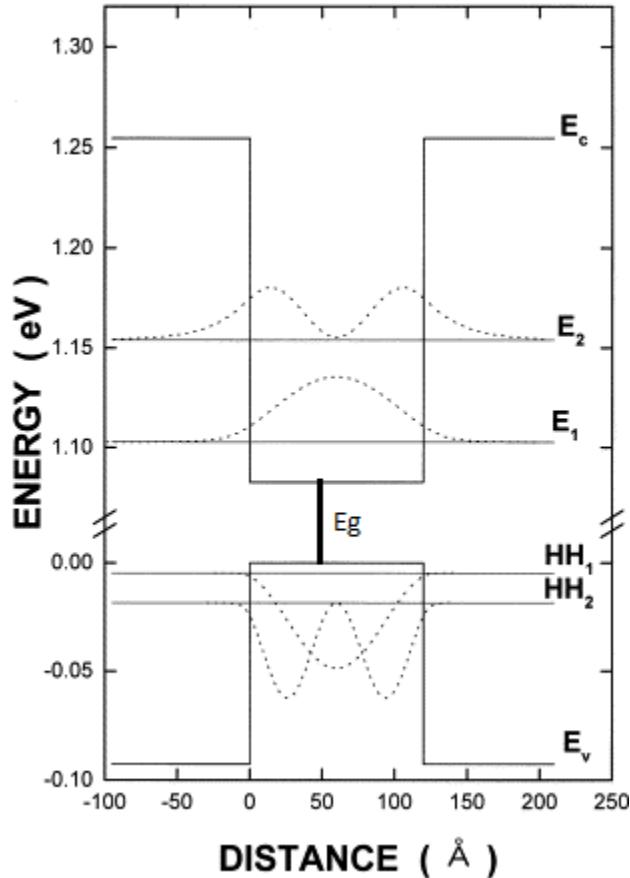
Figure 19.   Energy Gap of a Quantum Well [from Ref. 8]

The equation of a quantum-energy gap is a function of how thick is the well,

$$E_{QW} = E_g + \frac{\hbar^2 \pi^2}{2m_e L^2} + \frac{\hbar^2 \pi^2}{2m_h L^2} \tag{40}$$

and if we use reduced mass, the equation becomes

$$E_{QW} = E_g + \frac{\hbar^2 \pi^2}{2m_r L^2}, \text{ where } \frac{1}{m_r} = \frac{1}{m_e} + \frac{1}{m_h} \tag{41}$$

24

C.   SCHRÖDINGER EQUATION SOLUTIONS

1.   Infinite, Delta Function and Finite Well

To study quantum mechanics, we introduce the infinite well.
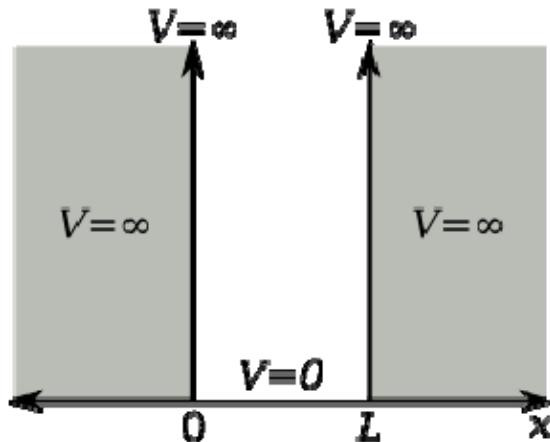
Figure 20.   Infinite Well [from Ref. 7]

Outside the well, the potential energy of the system V is equal to infinity. Inside the well, it is equal to zero.
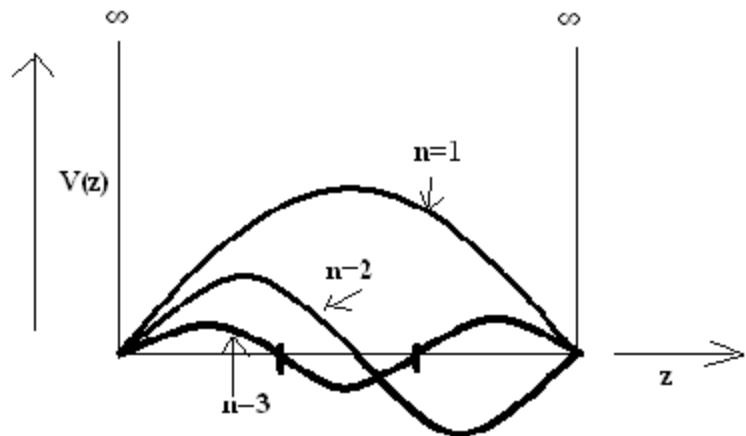
Figure 21.   First Energy Levels of Infinite Well [from Ref. 7]

In case the potential is different from zero we use two ways to solve the Schrödinger equation; the algebraic method, using ladder operators and factoring the Hamiltonian, and the power-series method.

In case the potential is zero (free particle), the general solution to time dependent is still a linear combination of separable solutions [7].

Borrowing some terms from classical mechanics, we can describe situations concerning the Schrödinger equation. The terms we use are "scattering" and "bound" states. Actually, they are clearer in quantum mechanics, because what matters is where the potential is. Inside the well is the bound state, and outside, the scattering state.

The Dirac delta function can describe the potential of a well and can substitute the potential of the Schrödinger equation.

Scattering states are not so easy to describe mathematically, due to approximations. We can only talk of probabilities, where the higher the energy, the larger the transmission probability. The importance of quantum scattering is that it describes a very important phenomenon in modern physics called tunneling. This phenomenon appears when a particle approaches a potential barrier. At E>>V we have total transmission, and at E<<V, total reflection.

A finite square well is similar to a delta-function well where bound and scattering states exist.
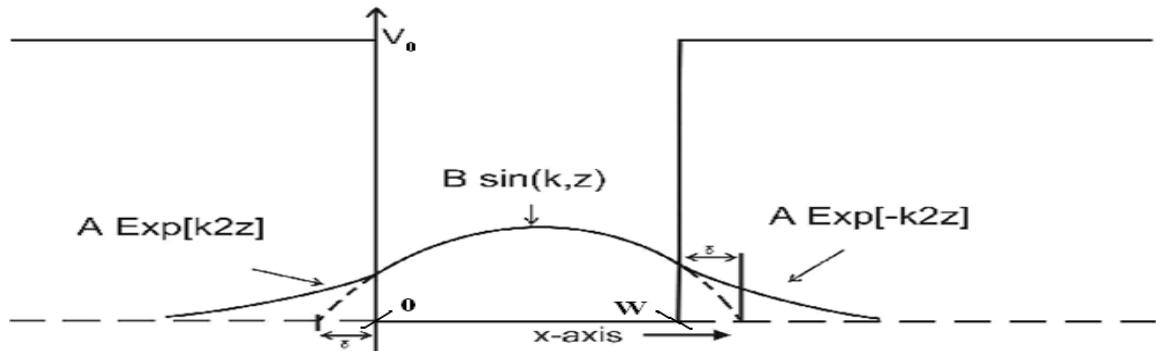
Figure 22.   Finite Potential Well [from Ref. 7]

26

2. Multiple and Asymmetric Well Systems

Quantum physics and new technologies demand designing and fabricating heterostructures more complex than one single well. These are multiple quantum well and asymmetrical well systems.

The general solution to multiple quantum wells becomes more complex as the number of wells increases or other characteristics change, such as depth and height V. Matrix forms give the probability interpretation of wave function.
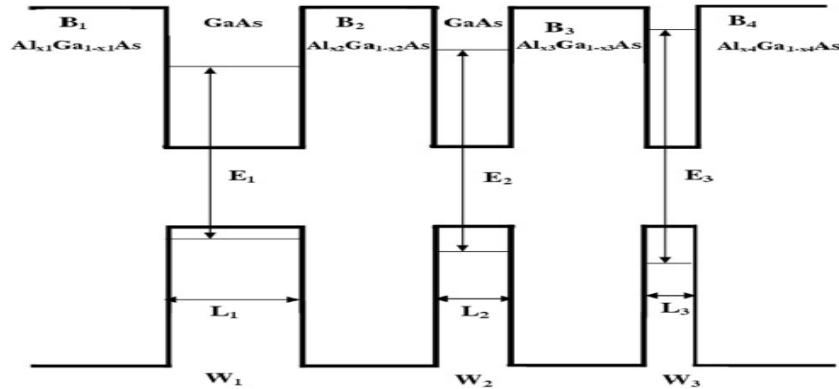
Figure 23.   Multiple GaAs AlGaAs Well [from Ref. 7]

When at a multiple quantum well the height barrier V differs from well to well, it is called asymmetrical. This becomes more complex on solving the Schrödinger equation, because transfer matrices should be established.
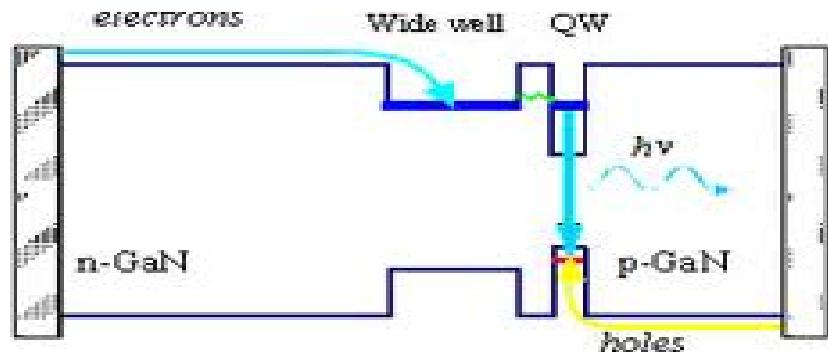
Figure 24.   Asymmetrical Well [from Ref. 7]

3. Barriers

The opposite structure to a potential well is a barrier. The characteristic that contrasts with a well is the larger bandgap. Barriers between a quantum well will trap or confine the electrons along one direction and be able to be collected from the material with the lower bandgap. The extraordinary phenomenon that happens in this area is that electrons that were created with even smaller energy than the potential height of the barrier have a probability larger than zero to pass through the barrier and contribute to the current flow. This is called quantum-mechanical tunneling, and the probability is called the transmission coefficient, given by the following equation:

$$T(E) = \frac{1}{1 + \left(\dfrac{k^2 + \kappa^2}{2k\kappa} \right)^2 \sinh^2(\kappa L)}$$

(42)

Equation (64) is not valid for more than one barrier. In this case, the symmetry and continuousness of the barriers matter. The solution in this situation is to use the matrix-transfer technique, where the coefficients of all barriers are linked.

It becomes obvious that when barrier-height V increases, the transmission coefficient decreases.
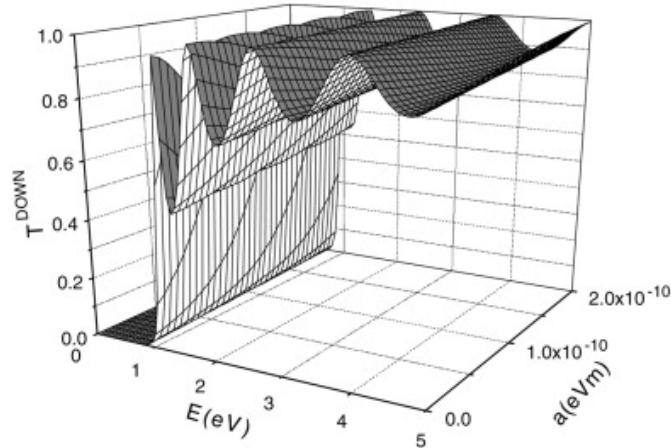
Figure 25.   Transmission coefficient [from Ref. 7]

28

Although the transmission coefficient is a very important factor, it is not measurable by itself.

To model current-voltage properties, we use the Fermi–Dirac distribution function to calculate the carriers that pass through the barriers, which is called resonant tunneling. Carrier distribution depends on temperature and barrier thickness. Carrier flow increases when temperature increases and when the barriers are thin enough.

4. 3D Infinite Potential Well

So far, we only have mentioned two-dimensional solutions to the Schrödinger equation. In real life, everything has three dimensions, so to be able to use quantum theory in applications, we must take under consideration all three spatial coordinates (x,y,z) and solve the Schrödinger equation. Using the equation of conservation of energy

$$E = K + V = \frac{p^2}{2m} + V \tag{43}$$

and by expressing p^2 as an operator we conclude with the following time-independent Schrödinger equation:

$$-\frac{\hbar^2}{2m}\left(\frac{\partial^2 \psi}{\partial x^2} + \frac{\partial^2 \psi}{\partial y^2} + \frac{\partial^2 \psi}{\partial z^2}\right) + V\psi = E\psi \tag{44}$$

THIS PAGE INTENTIONALLY LEFT BLANK

IV. SOLAR CELLS

A. SOLAR ENERGY

The sun is a four point six-billion-year-old star, with a mass of $2*10^{30}$Kg and radius of 700,000km. The surface temperature of the sun is estimated at 5.800° K; the temperature of the core is 14.000.000° K. The high temperature is a result of a nuclear-fusion reaction where fusing hydrogen releases 6.7% of the fused mass as energy, corresponding to $4.3*10^{3}$Kg/s. As sunlight passes through the earth's atmosphere, photons either scatter off water vapor, dust, smoke, and various particles, are absorbed by certain components of the atmosphere, or are reflected in the clouds and dissipated to the ground. A portion of the scattered radiation reaches the earth's surface and the rest diffuses into space. Thus, three components of incident solar radiation reach the surface: direct or immediate, diffused, and that which is reflected from the ground.

The sun radiates energy from its outer layers to the space allocated to all regions of the electromagnetic spectrum. It emits electromagnetic radiation in the infrared, visible, ultraviolet, X, and γ-ray spectra and emits particle radiation through the solar wind. Each of these radiations carries information concerning phenomena that occur in different layers of the sun. The solar spectrum is complex, with intense, continuous background punctuated by a few thousand dark and bright lines of various intensities. Fraunhofer first studied this reality, and the phenomenon bears his name. The configuration of the light spectrum emitted by the sun is usually fitted by the radiation of a black body temperature of about 5800° K. The energy distribution of the electromagnetic spectrum at each wavelength in the useful range of the spectrum is illustrated in Figure 27. The conversion of solar energy is determined by the detailed spectral distribution of the radiation, since the electrons that absorb energy to create a potential

31

difference have quantized energy levels. Therefore, the absorption of radiation is not immediate for any frequency.
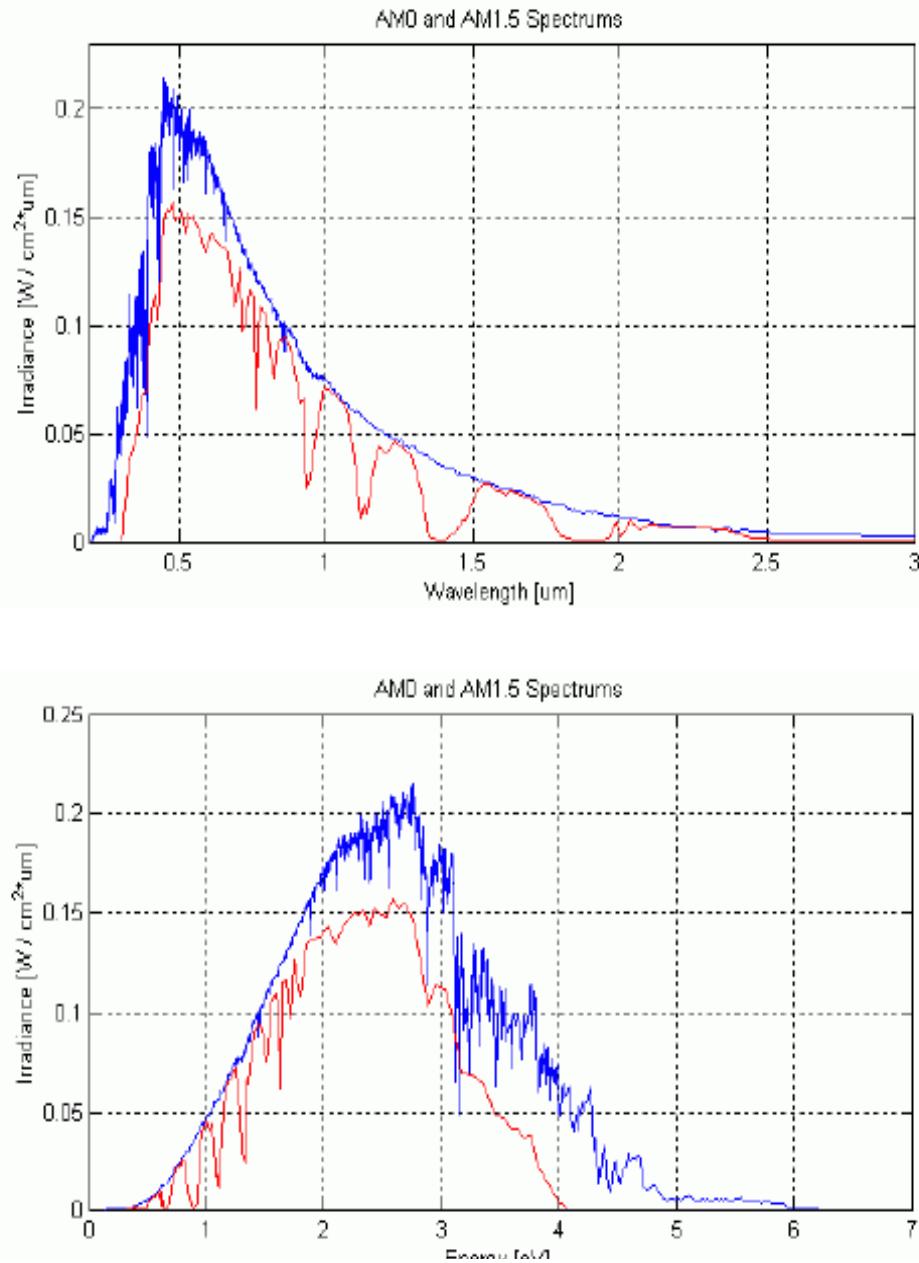
Figure 26.   AM0 and AM1.5 Spectrums [from Ref. 8]

The sunlight that reaches the earth has a very complicated spectral distribution. The most power is in the visible spectrum.

In Figure 27, we see two spectra, AM0 and AM1.5. The first is used for space applications and the second for terrestrial. Both were calculated using Planck's radiation law,

$$l(\lambda, \mathrm{T}) = \frac{2\pi c^2 h}{\lambda^5} \frac{1}{e^{hc/\lambda kT} - 1} \tag{45}$$

B.   FUNDAMENTALS

In the 1950s, the first efforts were made to convert solar radiation that reaches the earth into electrical energy. The amount of this energy is about 0.1353W/cm^2, and after passing the atmosphere is about 0.100W/cm^2. A pn junction as described in Chapter II was used to absorb this energy. The same junction, though more sophisticated, is still used. The goal is to achieve as much efficiency as possible with low-cost materials and technics. That is the reason we now mostly use GaAs and its alloys. GaAs has 1.42eV bandgap and, as we have described, can produce current from a photon, which has to have energy larger than 1.42ev, meaning a wavelength smaller than 875nm.

$$\lambda = hc / E \tag{46}$$

To take advantage of the whole spectrum, we use more than one material, with different bandgaps:
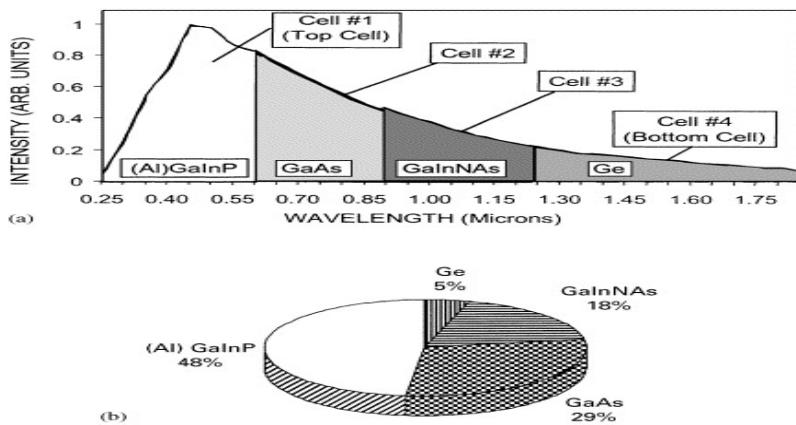
Figure 27.   Solar Cells as a Function of Wavelength [from Ref. 8]
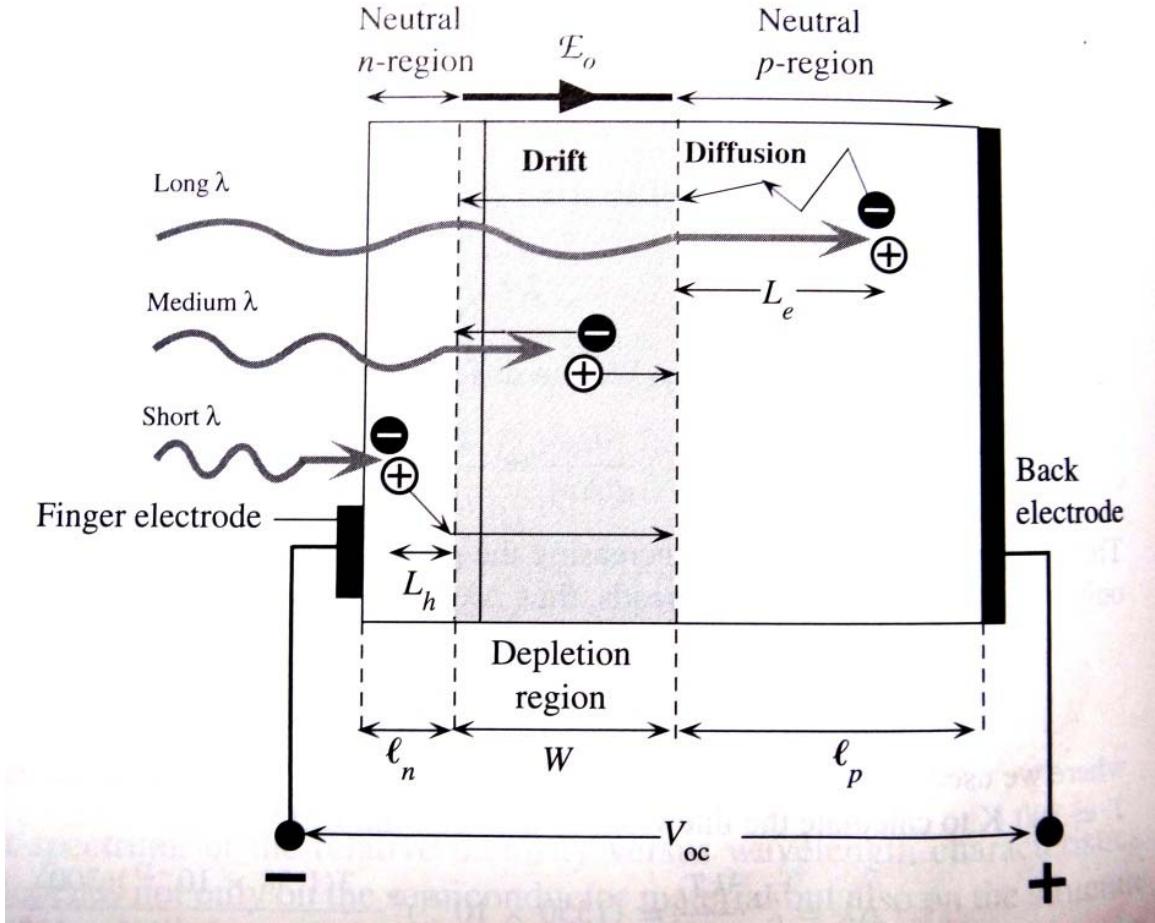
Figure 28.   Solar Cells: Principle of Operation [from Ref. 8]

In Figure 29, we see the principle of operation of a solar cell. The absorption of photons and the electron-hole pair (EHP) photogeneration happens mostly inside the depletion region, W, and the p-side. That charges negatively the n-side, creating an open circuit between the two regions. Not every EHP photogeneration contributes to the photovoltaic effect, but only those created in the minority carrier, diffusion length L_e, where

$$L_e = \sqrt{2D_e \tau_e} \tag{47}$$

and D_e is the diffusion coefficient and τ_e the recombination lifetime.

The remaining photo-generated EHPs are lost in recombination. This is the reason that at the bottom of the cell, the p-type semiconductor is chosen where electrons are the minority carriers. The current collected at the electrodes is called photocurrent. This current does not depend on the voltage of this junction, as there is always some. The voltage is the product of the photocurrent. In addition, there is diode current I_d, so the total current is given by the equation,

$$I = -I_{ph} + I_o \left[\exp\left(\frac{eV}{nkT}\right) - 1 \right] \tag{48}$$

where

$$I_d = I_o \left[\exp\left(\frac{eV}{nkT}\right) - 1 \right] \tag{49}$$

This produces the fundamental I–V curve
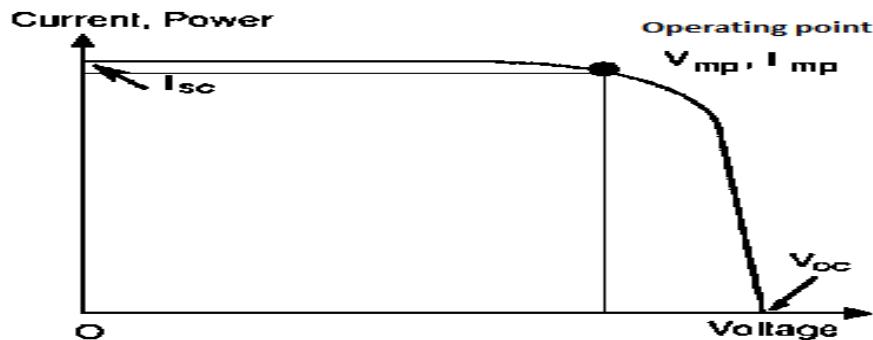
Figure 29.   I–V curve

The point that satisfies Equation 72 and Ohm's law is the operating point. This point and the fill factor have great importance, because they show how close to the ideal situation is our curve

$$FF = \frac{I_{mp} V_{mp}}{I_{sc} V_{oc}} \tag{50}$$

The solar cell has, besides the internal mechanism of producing current, other layers.

35
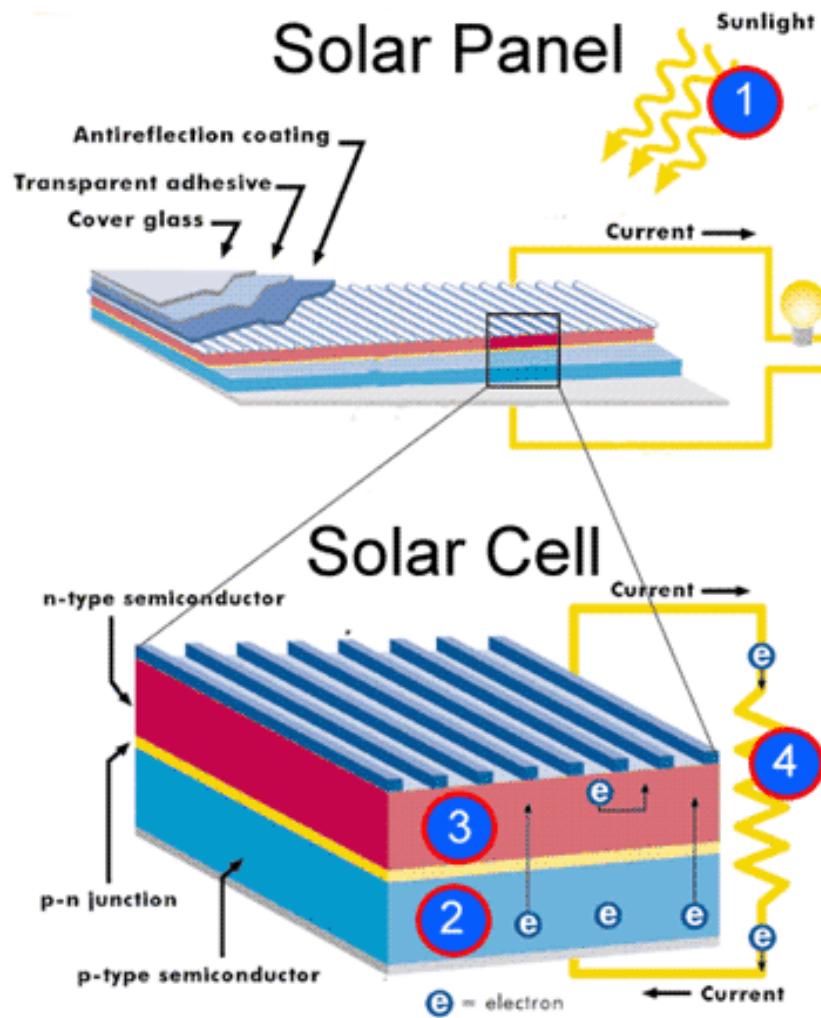
Figure 30.   Complete solar cell

As we see in Figure 31, finger electrodes are deposited on the n-side, and from there we collect the photocurrent. Also a thin antireflective coating reduces the reflected photons and allows more light to enter the device. Light follows Snell's law,

$$n_2 \sin \theta_2 = n_1 \sin \theta_1 \tag{51}$$
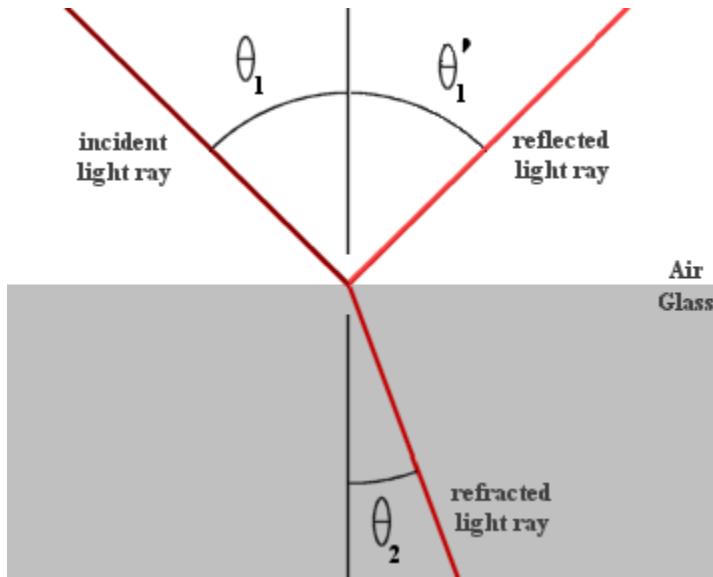
Figure 31.   Snell's law [from Ref. 2]

where n_2 is the index of refraction of the solar-cell coat and θ_1 the angle at which light falls on the cells. Obviously, we do not want any reflected light rays at the top of the cell, but would like a total reflection at the bottom, as it will allow more electron-hole-pair photogeneration.

C.   MULTIJUNCTION SOLAR CELLS

How a solar cell works is very similar to light-emitting diode (LED) operation, but exactly reversed. Nevertheless, LEDs achieve efficiencies of over 90%, whereas solar cells hardly reach 40%. The reason is that solar cells have not been able to take advantage of the whole spectrum of sunlight. This problem is being attacked by using multiple solar cells with varying bandgaps, stacked one atop the other. This allows converting photons of different wavelengths to photocurrent. The cells are stacked so that the highest bandgap material is on top, continuing to the bottom with materials of decreasing bandgap. This achieves higher efficiencies because higher-bandgap materials receive the highest solar radiation, which decreases as photons pass through the inner cells. Between cells we put low-energy pass filters so that the reflection threshold of

37

each filter is the bandgap of the cell above. This prevents luminescent photons from being emitted for energies different from those with which the photons from the sun are received in each cell [8]. The following table shows how efficiency differs from single to multijunction solar cells.

Cell	Efficiency [%]	Area [cm^2]	Intensity [suns]	Spectrum	Description
GaAs	25.1 ± 0.8	3.9	1	Global	Kopin, AlGaAs window
GaAs (thin film)	23.3 ± 0.7	4.0	1	Global	Kopin, 5-mm
GaAs(poly)	18.2 ± 0.5	4.0	1	Global	Res. Triangle Inst. (RTI) Ge substrate
InP	21.9 ± 0.7	4.0	1	Global	Spire, epitaxial
GaInP/GaAs	30.3	4.0	1	Global	Japan Energy
GaInP/GaAs/Ge	28.7 ± 1.4	29.93	1	Global	Spectrolab
Si	24.7 ± 0.5	4.0	1	Global	UNSW, PERL
GaAs	27.6 ± 1.0	0.13	255	Direct	Spire
GaInAsP	27.5 ± 1.4	0.08	171	Direct	NREL, ENTECH cover
InP	24.3 ± 1.2	0.08	99	Direct	NREL, ENTECH cover
GaInP/GaAs/Ge	32.4 ± 2.0	0.1025	414	Direct	Spectrolab
GaAs/GaSb	32.6 ± 1.7	0.053	100	Direct	Boeing, four-terminal mechanical stack
InP/GaInAs	31.8 ± 1.6	0.063	50	Direct	NREL, three-terminal, monolithic
GaInP/GaAs	30.2 ± 1.4	0.103	180	Direct	NREL, monolithic
Si	26.8 ± 0.8	1.6	96	Direct	Sunpower, back contact

Table 3.   Solar-Cell Efficiency Table [from Ref. 8]

If we look closely at this table, we will notice that the leading solar cell at this moment is the GaInP/GaAs/Ge solar cell. There were many studies on this particular multijunction solar cell, and more that are in progress. The reason is that the materials that the cell consists of are lattice matched and cover a wide range of the solar spectrum.
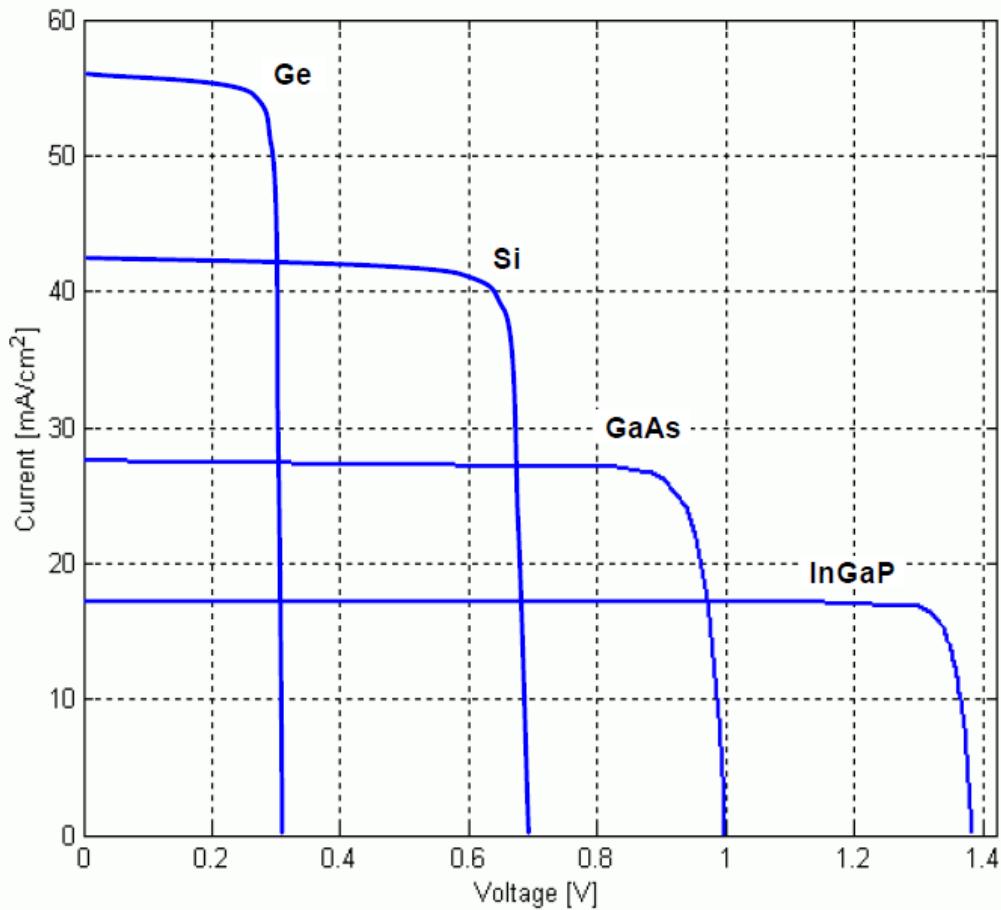
Figure 32.   I–V Curves [from Ref. 1]

Ge is the cheapest product and produces the highest current, because it absorbs most of the spectrum, and gives the smallest voltage. For this reason, it is usually put at the bottom of the solar cell as substrate.

GaAs is also a cheap material. Its properties (bandgap) are somewhere between Ge and InGaP. It is usually put in the middle.

Finally, InGaP is an expensive material that produces maximal voltage. Because of its bandgap, it absorbs the highest energy photons and it is usually put at the top of the solar cell.

Stacking them yields the following structure.
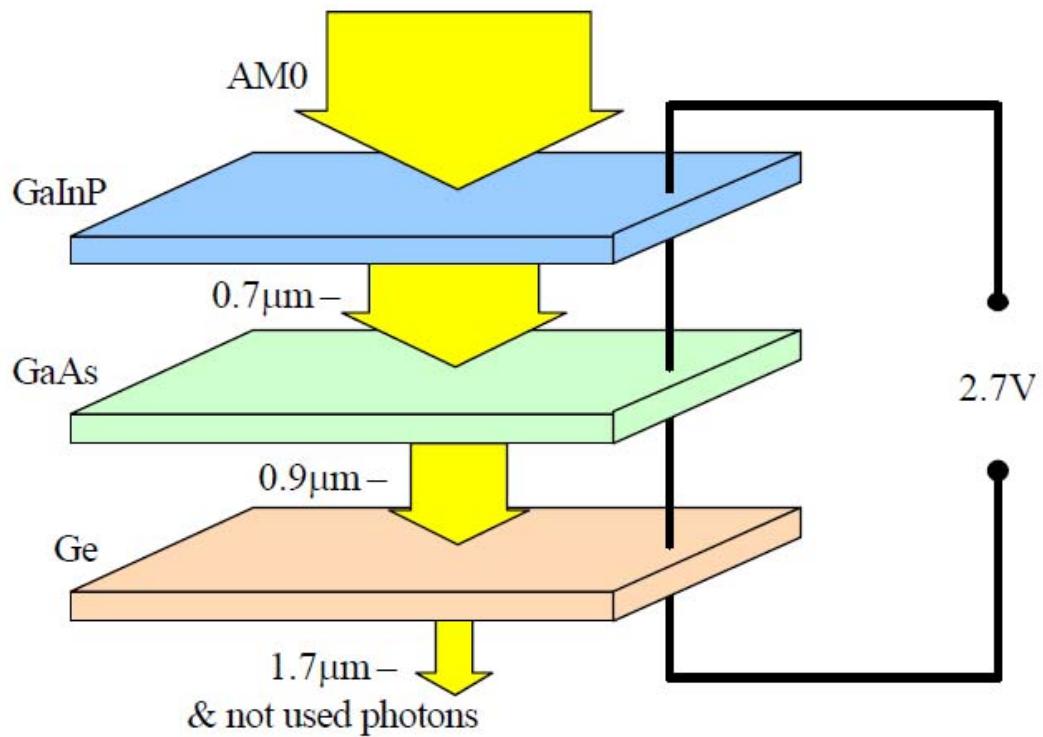
Figure 33.   Multijunction solar cell [from Ref. 1]

Great efforts have been made to simulate such a solar cell using Silvaco Atlas. The first and most important was made by a Panos Michalopoulos [1], followed by the important the work of Michael Hideto Tsutagawa [9], who improved the initial solar cell. The latter worked mostly in the improvement of dual-junction cell GaAs/InGaP. This was accomplished by increasing the thickness of both cells until the current is chocked and by keeping doping to realistic levels. Tsutagawa added the Ge cell, which resulted in a champion solar cell in which structure, characteristics, and I–V curve were as follows:

Region	Layer	Material	Thickness	Doping
Top InGaP Layer	Window	n+ AlInP	0.01μm	$5e19cm^{-3}$
	Emitter	n+ InGaP	0.17μm	$4.64e17cm^{-3}$
	Base	p+ InGaP	0.63μm	$1e17cm^{-3}$
	BSF	p+ InGaP	0.01μm	$5e19cm^{-3}$
	Buffer	p+ AlInP	0.3μm	$1e18cm^{-3}$
Tunnel Junction	Tunnel Emitter	p+ InGaP	0.015μm	$8e18cm^{-3}$
	Tunnel Base	n+ InGaP	0.015μm	$1e19cm^{-3}$
Middle GaAs Layer	Window	n+ AlInP	0.01μm	$4.64e17cm^{-3}$
	Emitter	n+ GaAs	0.01μm	$4.64e15cm^{-3}$
	Base	p+ GaAs	3.87μm	$1e17cm^{-3}$
	BSF	p+ InGaP	0.01μm	$5e19cm^{-3}$
	Buffer	p+ GaAs	0.3μm	$7e18cm^{-3}$
Tunnel Junction	Tunnel Emitter	p+ GaAs	0.015μm	$8e18cm^{-3}$
	Tunnel Base	n+ GaAs	0.015μm	$1e19cm^{-3}$
Bottom Ge Layer	Window	n+ GaAs	0.05m	$7e18cm^{-3}$
	Emitter	n+ Ge	0.1μm	$3e18cm^{-3}$
	Substrate	p+ Ge	300μm	$3e18cm^{-3}$

Figure 34.   Champion Solar-Cell Structure [from Ref. 1]
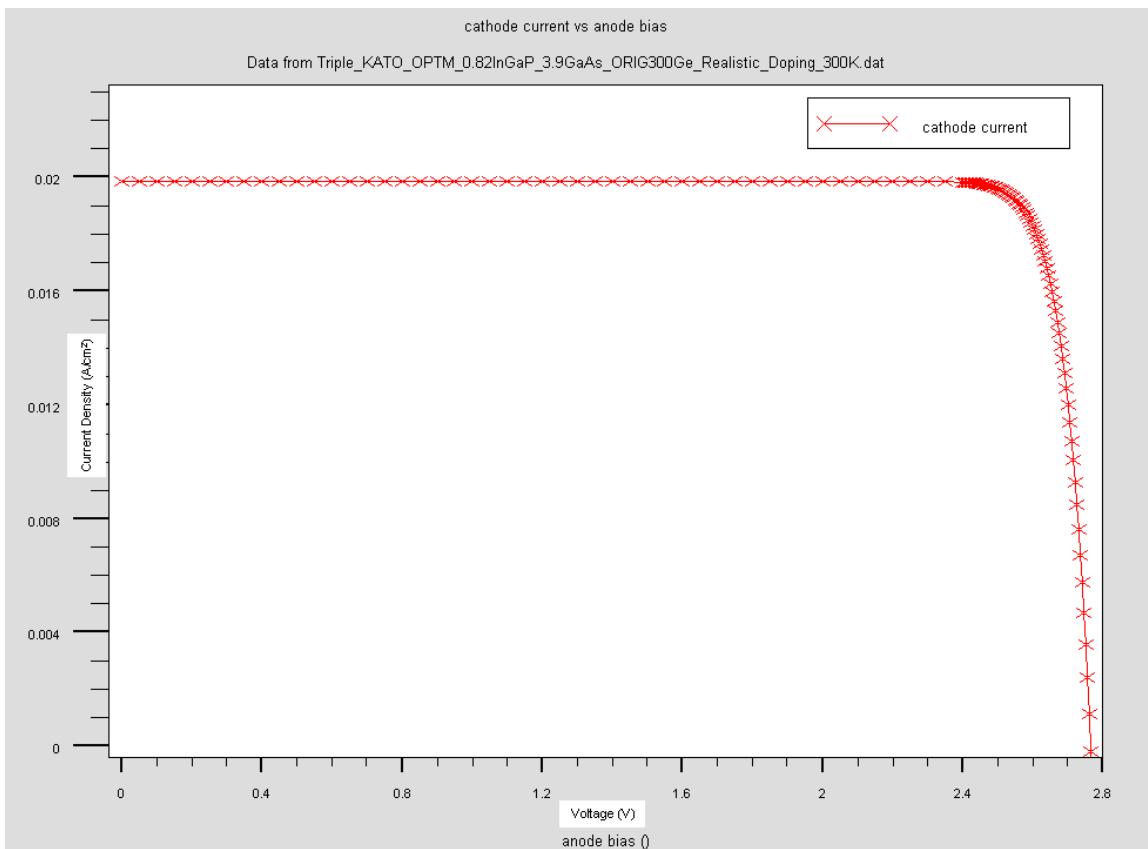
Figure 35.   Champion Solar Cell I–V Curve [from Ref. 9]

Parameter	Silvaco Model
Voc (V)	2.76425
Jsc(ma/cm^2)	19.85310
Vmax (V)	2.52500
Jmax(ma/cm^2)	19.44190
Pmax(mW/cm^2)	49.09080
Fill Factor	89.45%
Efficiency	36.28%

Table 4.   Champion Solar-Cell Specifications [from Ref. 9]

D. NANOSTRUCTURES

1. Introduction

Although the multijunction solar cell is at the forefront of present technology, it has two main disadvantages. Because it is very expensive to build, it is used only in space applications, as terrestrial uses would be prohibitively expensive. Secondly, it seems to have reached its limits of performance, unless something revolutionary is discovered or invented. Many researches are turning to different solar-cell structures as a result. One alternative is nanostructures, which are much easier to build, less expensive, and seem very promising. Multiple energy levels can be present in nanostructures and they can promote the existence of multiple absorption paths, in such a way that one photon generates more than one electron-hole pair [10]. Their great advantages are that they can achieve broader absorption rates and transport properties, introduce variable bandgaps, and have no light degradation.

2. Building a Nanostructure

New technology and growing techniques such as molecular-beam epitaxy (MBE), metal organic-chemical vapor deposition (MOCVD) and chemical-beam epitaxy (CBE) give the opportunity to deposit very thin films of semiconductors, which leads to dramatic behavioral changes. These films may have the thickness of a single atomic layer and be deposited over other materials. This development would have no result if it were not combined with modern physics and quantum mechanics, where the motion of electrons due to dimensionality reduction can be described. The first attempt began in 1974, when Dingle demonstrated quantum wells experimentally. Other forms of nanostructures are quantum wires, where electrons are confined in two dimensions, as compared to quantum wells, where they are confined in one. Another form is quantum dots, where electrons are confined in all three dimensions.

43
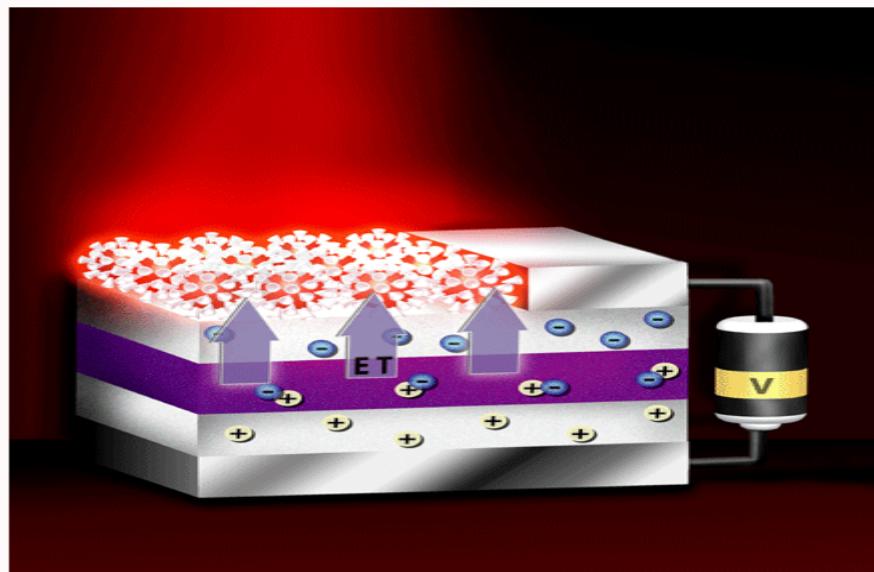
Figure 36.   Quantum Well [from Ref. 2]
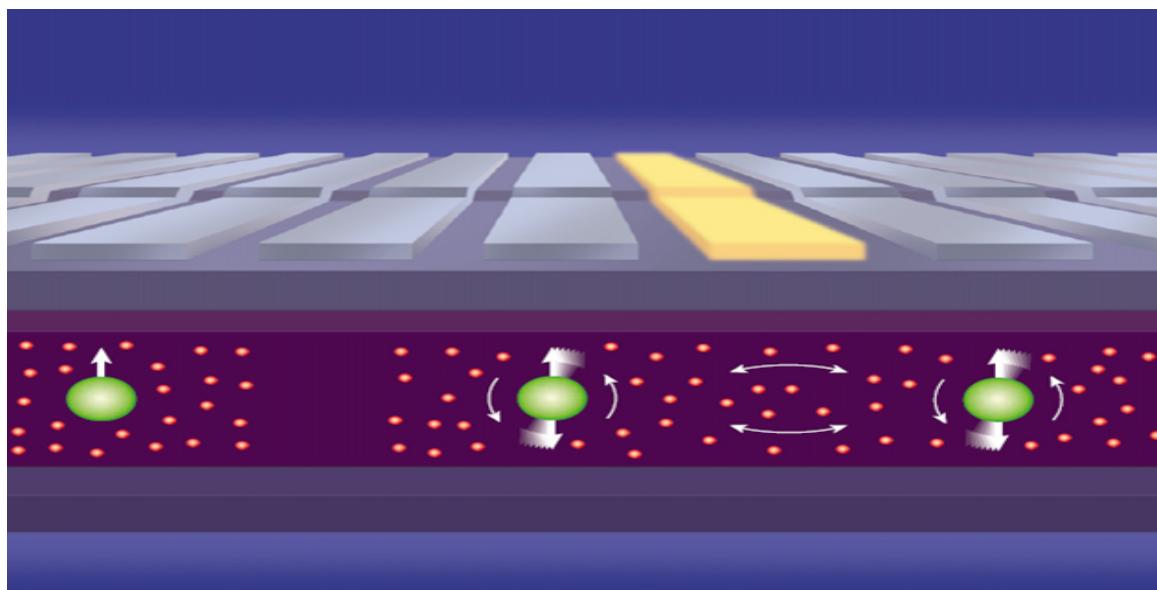
Figure 37.   Quantum Wire [from Ref. 2]
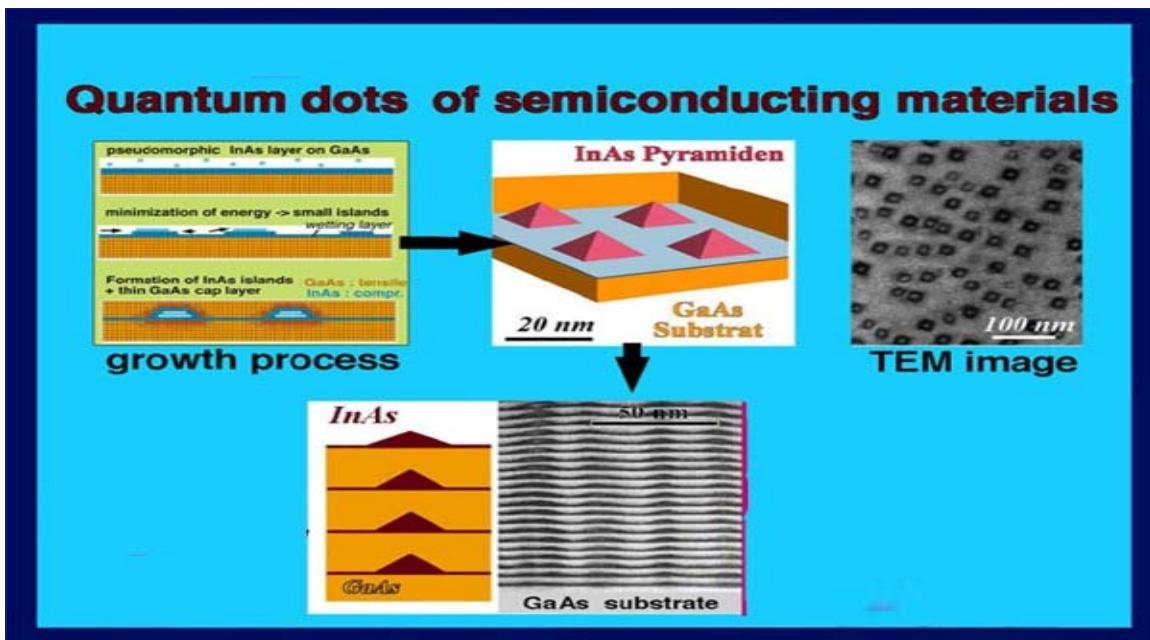
Figure 38.   Quantum Dot [from Ref. 2]
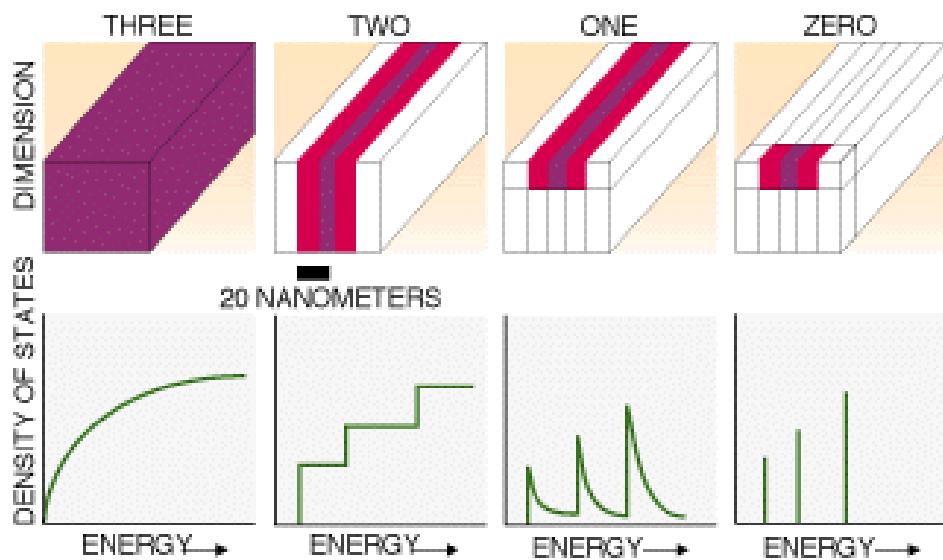
Figure 39.   Bulk, Quantum Well, Quantum Wire and Quantum Dot [from Ref. 7]

E. BUILDING AN INAS/GAAS QUANTUM WELL NANOSTRUCTURE

In theory, everything seems easily doable. All you have to do is to connect every piece in the puzzle. In reality, when it comes to building such a device, combining all the theories it is not only difficult, but most of the time unachievable. Such an example is an InAs/GaAs quantum-well nanostructure. Both InAs and GaAs have great properties, but it is very difficult to combine them.

Property \ Material	GaAs	InAs
Structure (All Cubic)	Zinc Blend	Zinc Blend
Lattice Parameter a_0 at 300K	0.5653 nm	0.605 nm
Density at 300K	5.318 g.cm^{-3}	5.69 g.cm^{-3}
LO Phonon Energy	285.0 cm^{-1}	. . . cm^{-1}
TO Phonon Energy	267.3 cm^{-1}	. . . cm^{-1}
Thermal Conductivity at 300 K	0.5 Wcm^{-1}K^{-1}	. . . W.cm^{-1}K^{-1}
Dielectric Constant (f=0 to f=RF)	12.5	14.6
Nature of Energy Gap Eg	Direct	Direct
Energy Gap Eg at 300 K	1.424 eV	0.36 eV
Intrinsic Carrier Conc. at 300 K	2.1×10^6 cm^{-3}	. . . cm^{-3}
Electron Hall Mobility at 300 K for n=1.3×10^{13} cm^{-3}	9200 cm^2/V.s	. . .cm^2/V.s
Electron Hall Mobility at 77 K for n=1.3×10^{13} cm^{-3}	2×10^5 cm^2/V.s	. . . cm^2/V.s
Ionisation Energy of Zinc Acceptor	30.6 meV	. . . meV
Hole Hall Mobility at 300 K for p=1×10^{14}cm^{-3}	ca. 400 cm^2/V.s	. . . cm^2/V.s
Hole Hall Mobility at 77 K for p=. . . cm^{-3}	ca. 7000 cm^2/V.s	. . . cm^2/V.s

Table 5.   Material Properties [from Ref. 7]

The greatest issue with these materials is lattice mismatch, which is approximately 6.8%. For InAs, the lattice constant is 6.0584 Å and for GaAs, 5.6533 Å. Manufacturing ultra-thin layers of InAs solves such a problem without exceeding the critical thickness of 3ML or 7 Å, growing in direction 001. That is because the strain tensor depends on the symmetry of the crystal. Structures with thicknesses greater than the critical thickness cause the strain to relax, creating dislocations and leading to a drop in system energy.
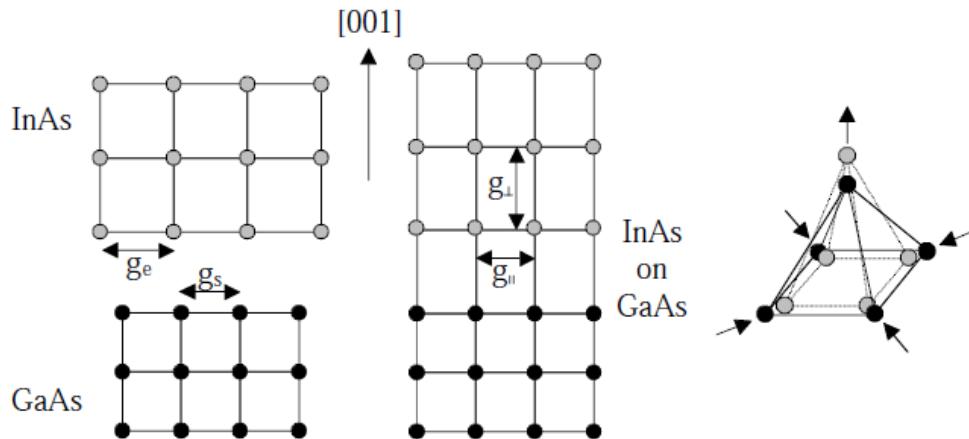
Figure 40.   GaAs InAs Formation

Matthews and Blakeslee model give the calculation of the critical thickness.
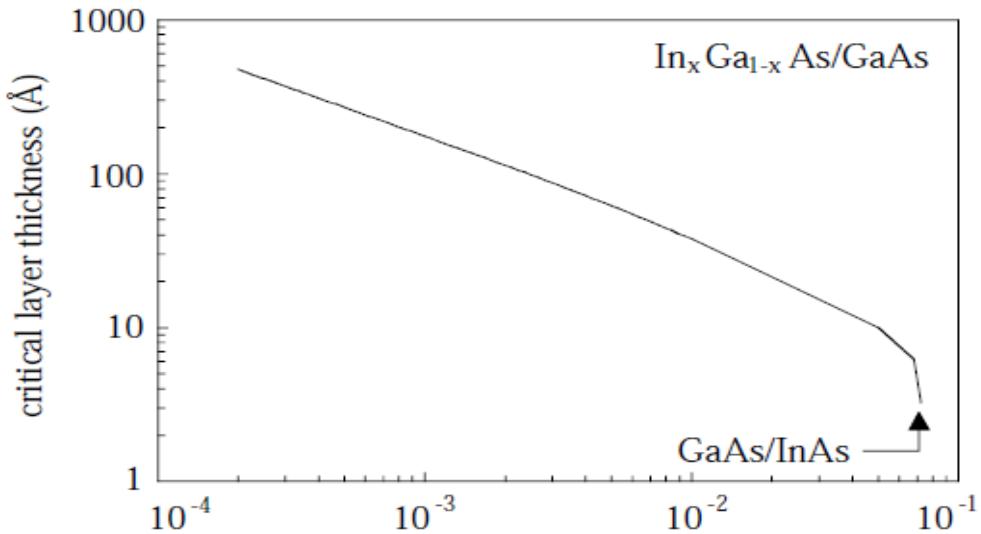
Figure 41.   GaAs InAs Formation [from Ref. 9]

Due to differences in electron affinity and bandgap of approximately 1 eV, the insertion of InAs in GaAs produces a strong confining potential in the conduction and valence band on the length scale of the lattice constant, which introduces bound-electron states in the GaAs bandgap [11]. By increasing the depth of the quantum well, the square-well model gives more than one bound state. Generally, InAs atoms substitute isoelectronic GaAs atoms and create a Coulomb potential, which provides more electrons in confined states. Experimentally, it has been found that the band offset is 0.9eV at the conduction band and 0.17eV at the valence band, but we must consider that it depends on dislocation.

Because of the significant big dielectric constant of GaAs, we achieve great photoluminescence efficiency. This arises from the recombination of excitons bound to InAs. The major part of electron-hole wave functions is located mainly within the well region and extends into the GaAs barrier. The population in the InAs layer affects all three absorption mechanisms, namely, the interband absorption by the subbands of the confined electron, hh, and lh state; the absorption by bound hh and lh excitons; and the absorption due to unbound exciton states, which are simultaneously present and which exhibit different changes under photoexcitation [12].

Ultrathin layers may solve the dislocation problem, but create one great disadvantage: low electron mobility. This leads to the conclusion that deep quantum wells are needed, so efforts are aimed at the problem of dislocation. Deeper wells have characteristics such as better wave-function confinement, smaller carrier density in barriers, higher leakage currents and slow transport between wells. However, the thickness has been such as to decrease the number of sub-bands and increase sub-band spacing [13]. Asahi Chemical Industry Co., LTD, gave a solution that is detailed in their paper, "Magnetoresistance Effect of InAs Deep Quantum Well Structures Grown on GaAs Substrates by Molecular Beam Epitaxy" [14]. The experiment was for

48

magnetoresistance effects, but what matters is the lattice-mismatch solution. They introduced a lattice-matched layer of AlGaAsSb to InAs that was grown with MBE on GaAs substrate. Generally, the scope was to grow a specially designed buffer layer on top of unsuitable substrate. If correctly designed, a graded buffer layer will confine the dislocations away from the active regions of the device, enabling the growth of high indium concentration $In_xGa_{1-x}As$ (x > 0.4) with low threading dislocation densities on GaAs substrates [13].
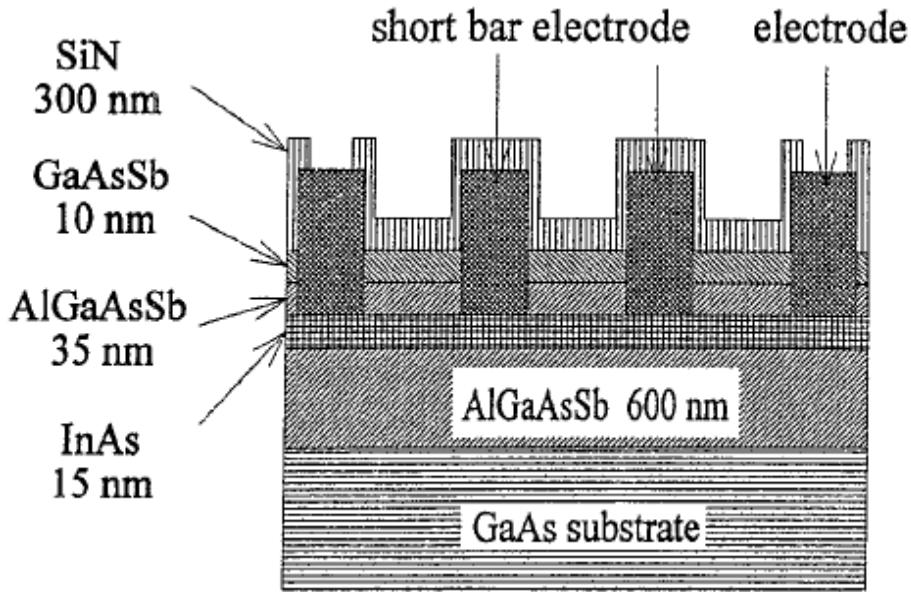
Figure 42.   InAs deep quantum-well structures grown on GaAs substrates [from Ref. 12]

Another perspective on building deep quantum wells is to try to improve the way that InAs stacks on GaAs. This effort is described in the paper "An Empirical Potential Approach to the Formation of InAs Stacking-Fault Tetrahedron in InAs/GaAs(111)" [15]. A very promising technique is tested, the stacking-fault tetrahedron (SFT), with very encouraging results. The InAs-SFT is more stable than coherently grown InAs on GaAs(111) beyond twenty-one monolayers (MLs), which are comparable with the critical film thickness of misfit dislocation generation [15].

49
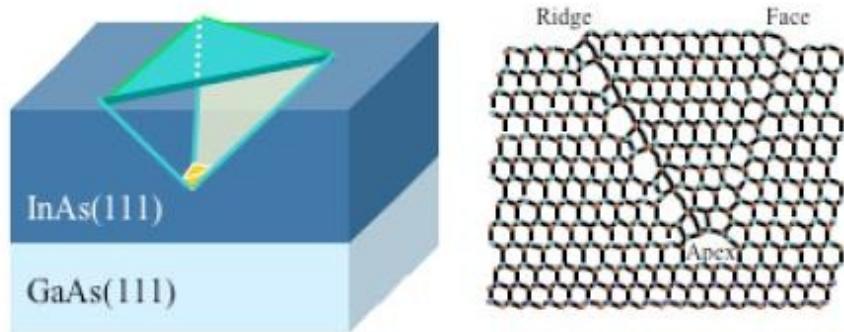
Figure 43.　InAs SFT with cross section [from Ref. 10]

Under this optical view, the cells were built such that the quantum-well thickness exceeded the critical thickness.

V. VIRTUAL WAFER FABRICATION – SILVACO ATLAS

A. INTRODUCTION

Due to their complexity and the many factors to be considered in their design, researchers prefer to fabricate rather than simulate solar cells. But although simulations are always questionable and must be verified, there will be always be a need, especially on the part of manufacturers, for software that simulates solar-cell design prior to production. The reason lies in the high cost of manufacturing, in which very expensive and unique materials are used to improve efficiency. One promising software for simulation is Silvaco Atlas, which was used with success in the Panos Michalopoulos thesis. Since then, there has been great progress in simulating more and more complex structures. In this thesis, Atlas is used for the first time to simulate quantum-well solar cells. There have been other simulations of quantum wells, but none for solar cells.
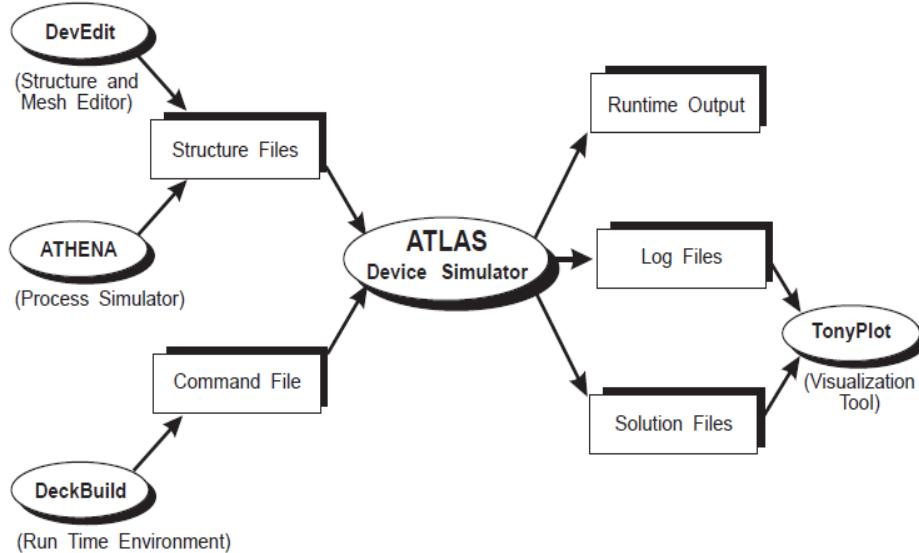
Figure 44.   Atlas [from Ref. 5]

This chapter gives a brief description of how Atlas works and a presentation of the code that was used in this research. The main order and framework for building code is shown in the following table.

Group		Statements
1. Structure Specification	———	MESH REGION ELECTRODE DOPING
2. Material Models Specification	———	MATERIAL MODELS CONTACT INTERFACE
3. Numerical Method Selection	———	METHOD
4. Solution Specification	———	LOG SOLVE LOAD SAVE
5. Results Analysis	———	EXTRACT TONYPLOT

Table 6.   Command Groups and Statements [from Ref. 5]

The order of command in this table must be followed. Failure to comply may lead not only to the termination of the program, but to incorrect operation and faulty results.

B.   SPECIFYING THE INITIAL MESH

The code starts by specifying the initial mesh of the structure. The mesh command specifies the location and the spacing of the lines. When building two-dimensional structures, x.mesh and y.mesh are introduced.

```
X.MESH LOCATION=<VALUE> SPACING=<VALUE>

Y.MESH LOCATION=<VALUE> SPACING=<VALUE>
```

Small values in these commands yield finer meshing and increased accuracy, but slower simulation. Large values yield the opposite. The optimal practice is to use larger values at the beginning to speed the simulation and to create as fine a mesh as possible towards the end. How large or small the value should be always depend on the size of each region, and is best expressed as a percentage of the total length of the x or y dimension. Although a two-dimensional structure is built, Atlas automatically considers a z direction of one micrometer's length. All units are in micrometers.
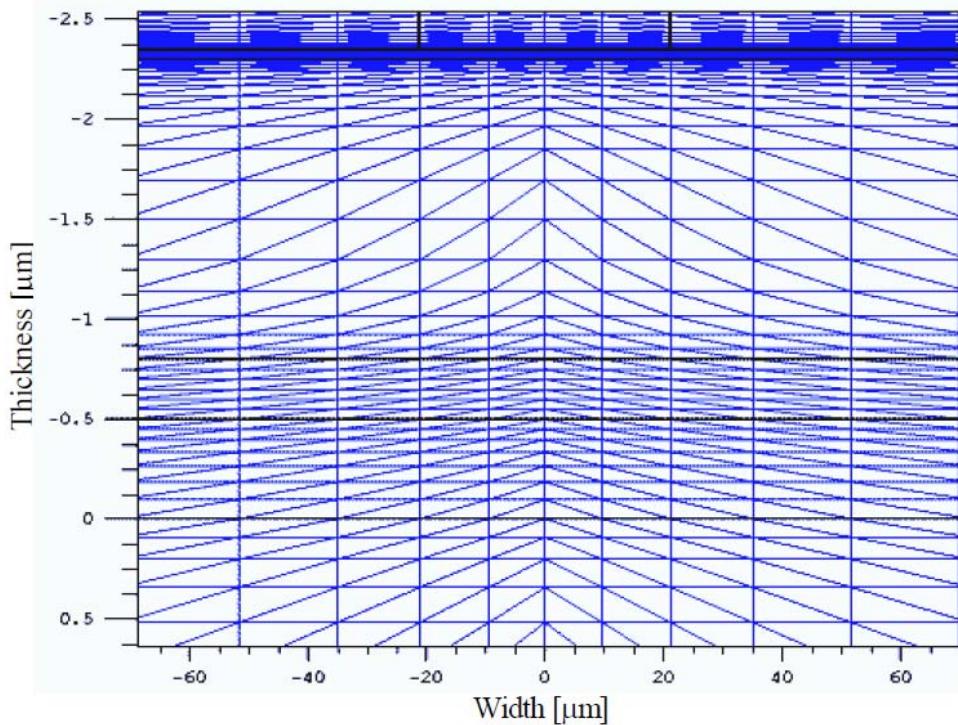
Figure 45.   Meshing [from Ref. 5]

When building the mesh in the x direction, we prefer to minimize the spacing at the center of the cell. At the y direction, mesh spacing usually changes in every region, depending always on the thickness of the region.

In this thesis, meshing in the x direction is specified by the following commands:

```
x.mesh loc=-250      spac=50
x.mesh loc=0         spac=10
x.mesh loc=250       spac=50
```

and in the y direction by the commands,

```
#Contact (100nm)
y.mesh loc=-0.15     spac=0.01
#Window (50nm)
y.mesh loc=-0.1      spac=0.005
#Emitter (100nm)
y.mesh loc=0         spac=0.01
#iGaAs (500nm)
y.mesh loc=0.5       spac=0.05
#wells (425nm)
y.mesh loc=0.925     spac=0.05
#iGaAs (75nm)
y.mesh loc=1.000     spac=0.05
#Base (300um)
y.mesh loc=300       spac=30.00
```

As can be noticed in the y direction, the spacing is 10% of the region's thickness

C. REGIONS

After specifying the mesh, the next step is to assign regions. Each region is described by a number, starting with one (1), and corresponds to a specific material. The maximum number of regions that Atlas allows is fifty-five (55). This is a limiting factor when building a multiple quantum-well solar cell, because in order to describe the quantum-well region of the solar cell, you have to introduce

many regions. Some papers say that twenty-five layers (or regions of quantum wells give the maximum performance, that is, almost half of the total allowed. The positions of the regions are specified in both directions by the commands x.min, x.max, y.min and y.max.

```
REGION NUM=<VALUE> MATERIAL=<VALUE> X.MIN=<VALUE>
X.MAX=<VALUE> Y.MIN=<VALUE> Y.MAX=<VALUE>
```

In this thesis, regions are set as follows:

```
#Vacuum
region   num=1   material=Vacuum   x.min=-250   x.max=-
100y.min=-0.25 y.max=-0.15
#Contact
region num=2 material=Gold    x.min=-100     x.max=100
y.min=-0.25    y.max=-0.15
#Vacuum
region num=3 material=Vacuum  x.min=100 x.max=250
y.min=-0.25    y.max=-0.15
#Window
region num=4 material=InAsP   x.min=-250     x.max=250
y.min=-0.15    y.max=-0.10
#Emitter
region num=5 material=GaAs    x.min=-250     x.max=250
y.min=-0.10    y.max=0.00
#iGaAs
region num=6 material=GaAs    x.min=-250     x.max=250
y.min=0.00     y.max=0.500
# well
region num=7 material=InAs    x.min=-250     x.max=250
y.min=0.500    y.max=0.525 name=well
region num=8 material=GaAs    x.min=-250     x.max=250
y.min=0.525    y.max=0.550
```

55

```
region num=9 material=InAs    x.min=-250    x.max=250
y.min=0.550    y.max=0.575 name=well
region num=10 material=GaAs    x.min=-250    x.max=250
y.min=0.575    y.max=0.600
region num=11 material=InAs    x.min=-250    x.max=250
y.min=0.600    y.max=0.625 name=well
region num=12 material=GaAs    x.min=-250    x.max=250
y.min=0.625    y.max=0.650
region num=13 material=InAs    x.min=-250    x.max=250
y.min=0.650    y.max=0.675 name=well
region num=14 material=GaAs    x.min=-250    x.max=250
y.min=0.675    y.max=0.700
region num=15 material=InAs    x.min=-250    x.max=250
y.min=0.700    y.max=0.725 name=well
region num=16 material=GaAs    x.min=-250    x.max=250
y.min=0.725    y.max=0.750
region num=17 material=InAs    x.min=-250    x.max=250
y.min=0.750    y.max=0.775 name=well
region num=18 material=GaAs    x.min=-250    x.max=250
y.min=0.775    y.max=0.800
region num=19 material=InAs    x.min=-250    x.max=250
y.min=0.800    y.max=0.825 name=well
region num=20 material=GaAs    x.min=-250    x.max=250
y.min=0.825    y.max=0.850
region num=21 material=InAs    x.min=-250    x.max=250
y.min=0.850    y.max=0.875 name=well
region num=22 material=GaAs    x.min=-250    x.max=250
y.min=0.875    y.max=0.900
region num=23 material=InAs    x.min=-250    x.max=250
y.min=0.900    y.max=0.925 name=well
```

```
#iGaAs
region num=24 material=GaAs   x.min=-250     x.max=250
y.min=0.925     y.max=1.000
#Base
region num=25 material=GaAs   x.min=-250     x.max=250
y.min=1.000     y.max=300.000
```

Figure 46.   Region Sructure GaAs InAs MQWs

D.   ELECTRODES

The next step is to specify where the current will be collected by the electrode command. The electrodes are located at top and bottom. When a multijunction cell is introduced, an electrode at the tunnel should also be introduced. The position parameters are similar to those in regions.

```
ELECTRODE NAME=<electrode name> <position_parameters>
```

In this thesis, electrodes are found only in the top and the bottom of the cell and they are described by the following commands:

```
electrode name=cathode top
electrode name=anode bottom
```

E.   DOPING

The following step is to specify the concentration of holes or electrons inside the semiconductors. The importance of doping was described in the previous chapter. Increased hole or electron concentration gives many advantages to materials. According to some experimental data, the doping limit is around 1e20; beyond that, many negative side effects appear. In Silvaco Atlas, usually there is no limit and side effects do not appear. Atlas allows the application of Gaussian doping in addition to uniform. Here we use the uniform version for the three regions with the following command:

```
doping uniform region=4  n.type    conc=1e19
doping uniform region=5  n.type    conc=2e18
doping uniform region=25 p.type    conc=1e18
```

F.   MATERIAL PROPERTIES

Continuing with the simulation, the code material properties are next to be defined. In Silvaco's library are preset basic material properties that can be modified and given desired values if, for example, there is new experimental data. The material properties described by the material command are the energy bandgap at 300 kelvin–Eg300, the dielectric constant (or permittivity), the electron affinity, electron and hole mobilities, and the conduction and valence band density of states. The material properties used in the present code are shown below.

```
#Vacuum
material material=Vacuum real.index=3.3  imag.index=0
```

```
#GaAs
material material=GaAs    EG300=1.42
PERMITTIVITY=13.1    AFFINITY=4.07
material material=GaAs    MUN=8800  MUP=400
material material=GaAs    NC300=4.7e17    NV300=7e18
material material=GaAs    sopra=Gaas.nk

# InAs
material material=InAs    EG300=0.36
PERMITTIVITY=15      AFFINITY=4.03
material material=InAs    MUN=30000 MUP=240
material material=InAs    NC300=8.7e16    NV300=6.6e18
material material=InAs    sopra=Inas.nk

# AlInP (=InAsP)
material  material=InAsP  EG300=2.4  PERMITTIVITY=11.7
AFFINITY=4.2
material material=InAsP MUN=2291 MUP=142
material material=InAsP NC300=1.08e20 NV300=1.28e19
#material material=InAsP sopra=Alinp.nk

# InGaP
material  material=InGaP  EG300=1.9  PERMITTIVITY=11.62
AFFINITY=4.16
material material=InGaP MUN=1945 MUP=141
material material=InGaP NC300=1.3e20 NV300=1.28e19
#material material=InGaP sopra=Ingap.nk
#Gold
material material=Gold real.index=1.2 imag.index=1.8
```

G.   MODELS

To describe the structure and pertinent phenomena as near to reality as possible, Silvaco provides models in five categories: carrier statistics, mobility, recombination, impact ionization, tunneling, and carrier injection. The models used in this thesis are the following:

```
models k.p fermi incomplete consrh auger optr print
models name=well k.p chuang spontaneous lorentz
```

These models are not described in the Silvaco Atlas manual, but in a recent example, which can be found online, in which an attempt to simulate quantum wells in GaN LED device is made.

H.   LIGHT BEAMS

Since light from the sun is responsible for power generation in a cell, and since the intensity, angle, polarization, spectrum, and other parameters differ depending on the application, a light beam description is required. I used a common statement that is used in many solar simulations and described by the following code:

```
beam  num=1     am1.5    wavel.start=0.21    wavel.end=4
wavel.num=50
```

That code can be translated as one beam, with 50 samples of wavelength between 0.21 to 4 micrometers, reaching the device on the surface of the earth.

I.   SOLVING AND DISPLAYING

So far, the purpose of the code has been first to specify the parameters of the materials used and second to use these materials to build a solar panel. With these steps completed, we now compute how this structure works under specified conditions and print out the desired results. Atlas uses three basic methods to calculate solutions: the Gummel, Newton, and Block. In this code, the Gummel method is used, which solves for each unknown, keeps other variables constant, and repeats until a stable solution is achieved.

The values that we are looking for from the computation are first to draw out the I–V curve and from there to calculate the short-circuit current density (Jsc), the open circuit voltage (Voc), the maximum power (Pmax), the maximum current (Jmax), the fill factor (FF) and the efficiency (Eff). The I–V curve is plotted by Atlas's Tonyplot tool, which is useful because it can give further information as long as a command inside the code is asking for structure.

Unfortunately, given the number and thickness of regions in this thesis' code, Tonyplot is unable to plot the structure—as Silvaco engineers stated would be true. As mentioned from the beginning of this thesis, this is the first attempt at simulating a multiple quantum-well solar cell with this software. The code is fully described in Appendix A and results are shown in the following table and figure.

Jsc	0.040912
Voc	0.955576
Pmax	0.0335872
Vmax	0.86
Jmax	0.0390549
FF	0.859128
Eff	0.335872

Table 7.   GaAs InAs MQWs Data
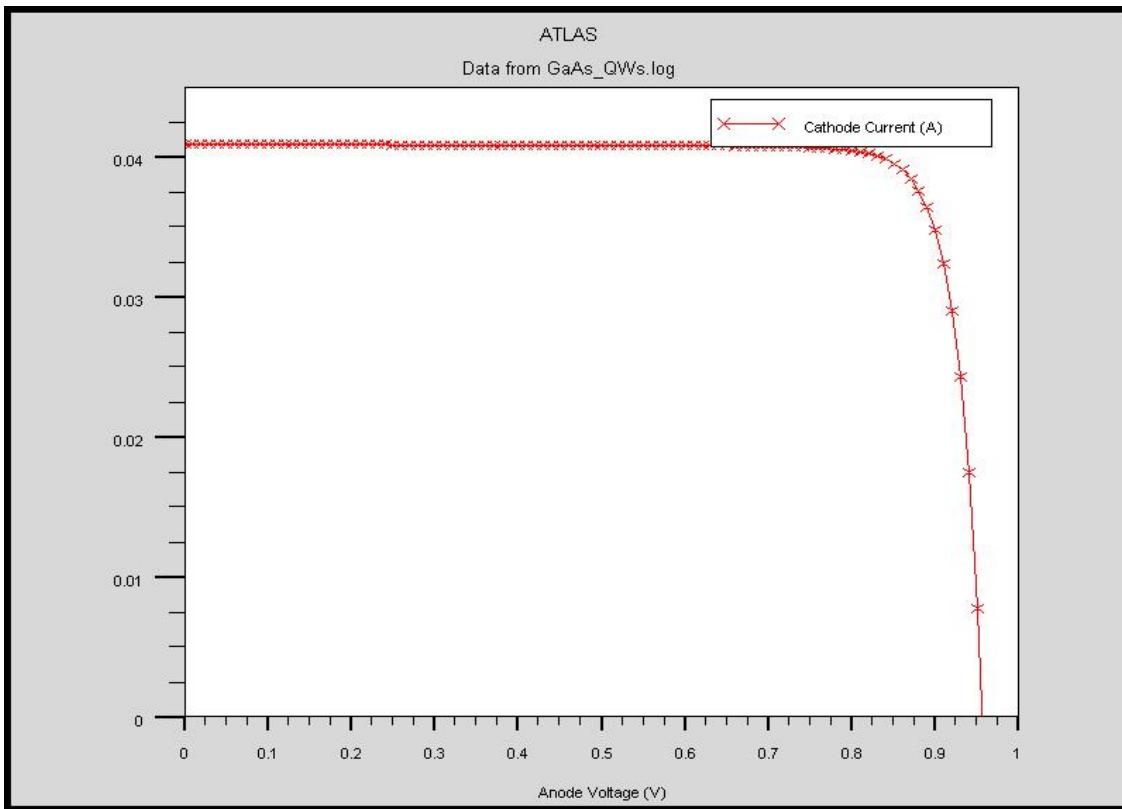
Figure 47.   I–V Curve GaAs InAs MQWs

Many efforts were made trying to decrease the depth of the wells to be as close as possible to critical thickness. The final, successful attempt is a cell structure with a 5nm well and barrier thickness. The cell had to be constructed from scratch, because when the attempt was made using the code in Appendix A, Atlas crashed. The new code has many similarities to the previous one, and one model was removed to be able to function. The new cell, which is less efficient but more realistic, is shown below, including the regions structure, I–V curve, and its specifications.
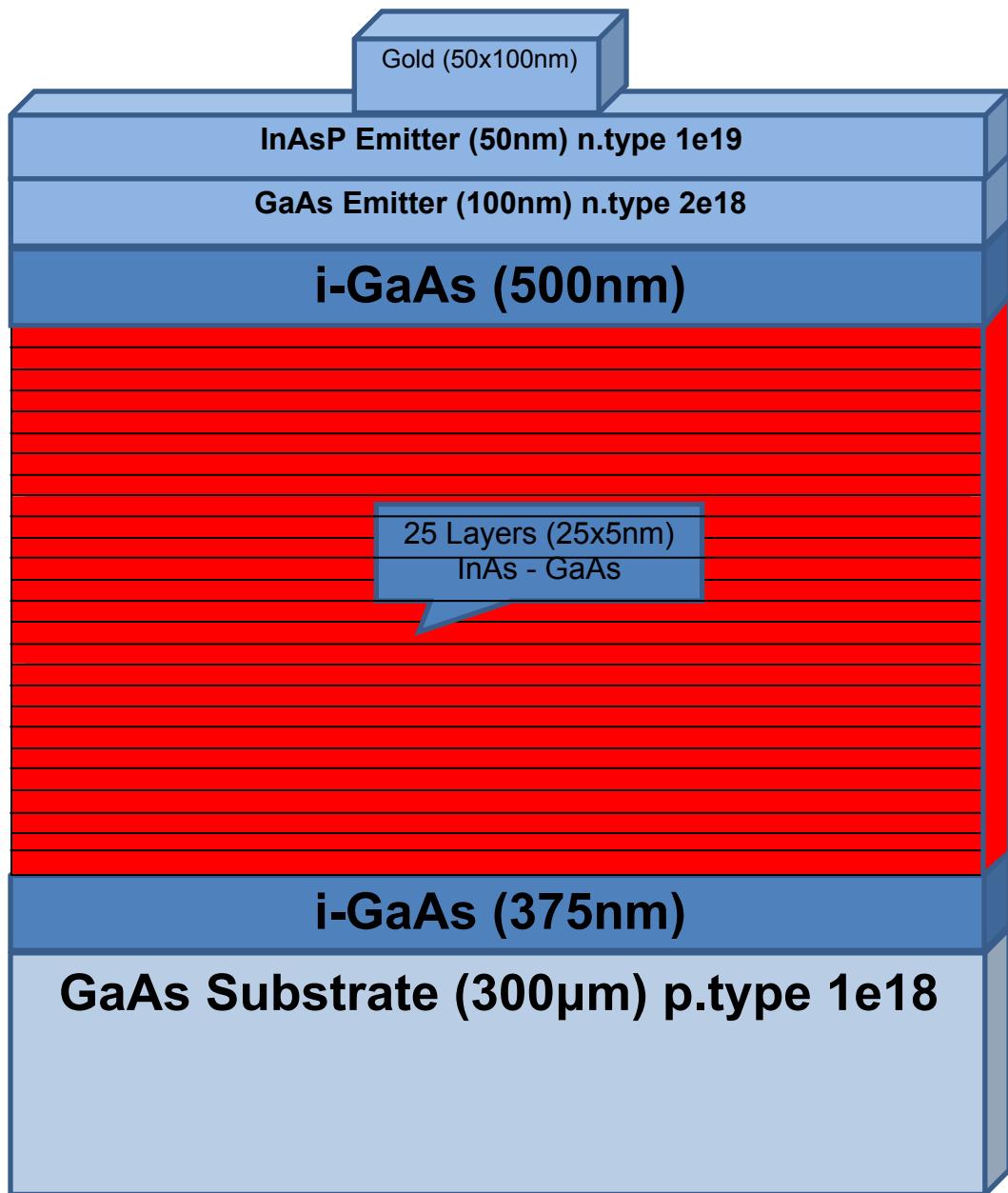
Figure 48.   Region Sructure GaAs InAs MQWs 5nm

Jsc	0.0336647
Voc	0.950253
Pmax	0.0274008
Vmax	0.85
Jmax	0.0322362
FF	0.856543
Eff	0.274008

Table 8.   GaAs InAs MQWs 5nm Data
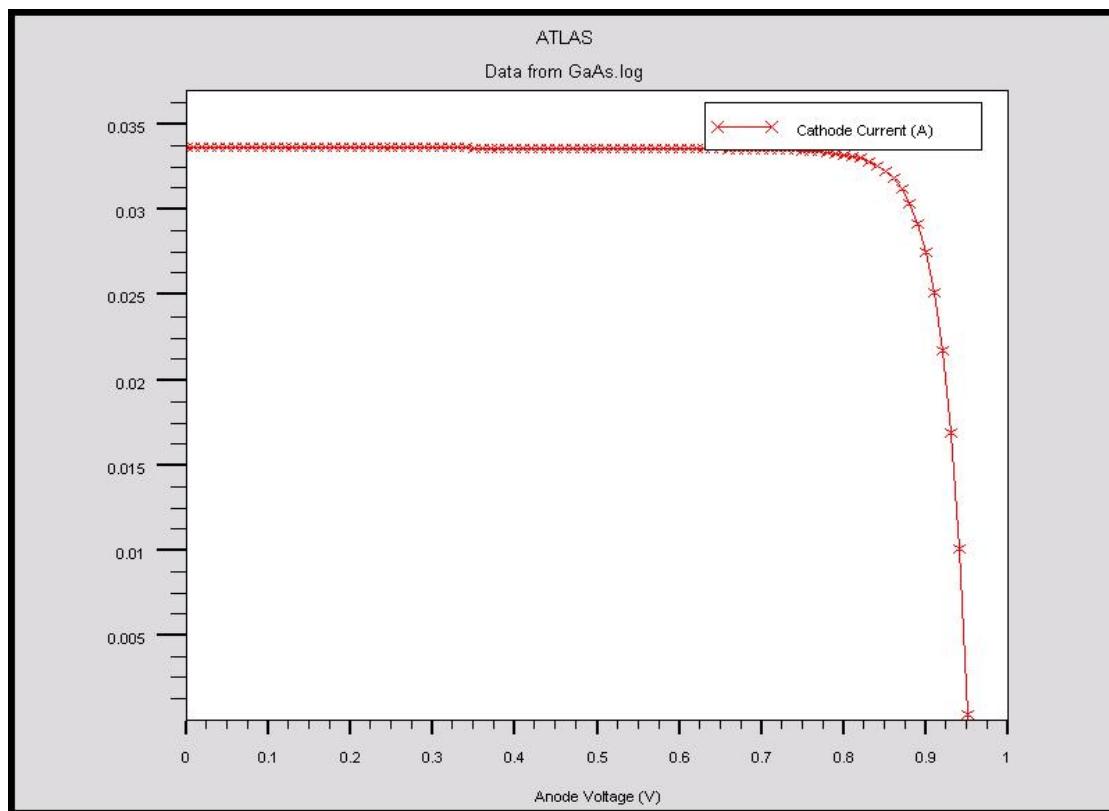
Figure 49.   I–V Curve GaAs InAs MQWs 5nm

THIS PAGE INTENTIONALLY LEFT BLANK

VI.   CONCLUSIONS AND RECOMMENDATIONS

A.   CONCLUSIONS

A novel code was presented for modeling and developing a new-generation, state-of-the-art solar cell. Many obstacles emerged in the Silvaco Atlas software while trying to design a multi quantum-well solar cell. Atlas has not been updated so as to be able to design such solar cells without problems. However, the results obtained are impressive, promising, and potentially of great value to photovoltaic researchers. This proposed simulation took an inexpensive, single solar cell with efficiency of 16% and upgraded it to 27% for a 5nm well thickness or 33% for a 25nm well thickness cell, according always to Atlas results. Unfortunately, because of the number and the thickness of regions involved, Atlas was not able to create a structure file in tonyplot, whence much useful information would be extracted. This code and its results are not experimentally proven, but it is hoped that a real model will soon be built to verify accuracy.

B.   RECOMMENDATIONS

Several approaches can be made to optimizing a solar cell, but the effort should focus in the area of quantum wells. The thickness of the intrinsic area and the position of the quantum wells inside this area should be tested and studied. Furthermore, if someone were to insert this cell inside a multijunction solar cell, he would, in the author's opinion, raise efficiency to levels that are now mentioned only in theoretical terms. Since this method has raised the efficiency of a single solar cell over 27%, it may, in a multijunction cell raise the efficiency from 38% to over 45%.

To conclude, Silvaco improvements to models and regions to create more stable codes would be very welcome. Models should be able to better describe

the mechanism inside a well, and for regions a new specification should be established that describes a quantum well or a quantum dot. Unless the region number is fixed, Atlas will not be able to simulate a multi-junction cell that includes multi-quantum wells, because it can only handle up to fifty-five regions—whereas, in the author's code, thirty were used for one cell alone.

APPENDIX A. ATLAS SOURCE CODE I

```
#LT EVANGELOS KOLETSIOS HN  *****DEC 2012*****

#This model is a novel Multi Quantum Well GaAs/InAs solar
cell using ORIGINAL parameters with dopant for increased
power.

#Code is based on Panos Michalopoulos GaAs solar cell code.


go atlas

#Definition of constants

#Mesh

#X-Mesh

#Y-Mesh

#Regions

#Electrodes

#Doping

#Material Properties

#Models

#Light Beams

#Solving


##############################

#MESHING

##############################
```

```
mesh width=200000

#X-mesh:  Surface=500 um2 = 1/200000 cm2

x.mesh loc=-250      spac=50

x.mesh loc=0         spac=10

x.mesh loc=250 spac=50


#Y-Mesh

#Contact (100nm)

y.mesh loc=-0.15     spac=0.01

#Window (50nm)

y.mesh loc=-0.1      spac=0.005

#Emitter (100nm)

y.mesh loc=0         spac=0.01

#iGaAs (500nm)

y.mesh loc=0.5 spac=0.05

#wells (425nm)

y.mesh loc=0.925     spac=0.05

#iGaAs (500nm)

y.mesh loc=1.000     spac=0.05

#Base (300um)

y.mesh loc=300 spac=30.00
```

```
###############################
#REGIONS
###############################
#Vacuum
region num=1 material=Vacuum  x.min=-250    x.max=-10
y.min=-0.25    y.max=-0.15
#Contact
region num=2 material=Gold    x.min=-100    x.max=100
y.min=-0.25    y.max=-0.15
#Vacuum
region num=3 material=Vacuum  x.min=100    x.max=250
y.min=-0.25    y.max=-0.15
#Window
region num=4 material=InAsP   x.min=-250    x.max=250
y.min=-0.15    y.max=-0.10
#Emitter
region num=5 material=GaAs    x.min=-250    x.max=250
y.min=-0.10    y.max=0.00
#iGaAs
region num=6 material=GaAs    x.min=-250    x.max=250
y.min=0.00    y.max=0.500
# well
region num=7 material=InAs    x.min=-250    x.max=250
y.min=0.500    y.max=0.525 name=well
```

```
region num=8 material=GaAs          x.min=-250     x.max=250
y.min=0.525    y.max=0.550

region num=9 material=InAs          x.min=-250     x.max=250
y.min=0.550    y.max=0.575 name=well

region num=10 material=GaAs         x.min=-250     x.max=250
y.min=0.575    y.max=0.600

region num=11 material=InAs         x.min=-250     x.max=250
y.min=0.600    y.max=0.625 name=well

region num=12 material=GaAs         x.min=-250     x.max=250
y.min=0.625    y.max=0.650

region num=13 material=InAs         x.min=-250     x.max=250
y.min=0.650    y.max=0.675 name=well

region num=14 material=GaAs         x.min=-250     x.max=250
y.min=0.675    y.max=0.700

region num=15 material=InAs         x.min=-250     x.max=250
y.min=0.700    y.max=0.725 name=well

region num=16 material=GaAs         x.min=-250     x.max=250
y.min=0.725    y.max=0.750

region num=17 material=InAs         x.min=-250     x.max=250
y.min=0.750    y.max=0.775 name=well

region num=18 material=GaAs         x.min=-250     x.max=250
y.min=0.775    y.max=0.800

region num=19 material=InAs         x.min=-250     x.max=250
y.min=0.800    y.max=0.825 name=well

region num=20 material=GaAs         x.min=-250     x.max=250
y.min=0.825    y.max=0.850
```

```
region num=21 material=InAs          x.min=-250     x.max=250
y.min=0.850     y.max=0.875 name=well

region num=22 material=GaAs          x.min=-250     x.max=250
y.min=0.875     y.max=0.900

region num=23 material=InAs          x.min=-250     x.max=250
y.min=0.900     y.max=0.925 name=well

#iGaAs

region num=24 material=GaAs          x.min=-250     x.max=250
y.min=0.925     y.max=1.000

#Base

region num=25 material=GaAs          x.min=-250     x.max=250
y.min=1.000     y.max=300.000


#############################
#ELECTRODES
#############################
electrode name=cathode top

electrode name=anode   bottom


#############################
#DOPING
#############################
doping uniform region=4  n.type    conc=1e19

doping uniform region=5  n.type    conc=2e18

doping uniform region=25 p.type    conc=1e18
```

```
##############################

#MATERIAL PROPERTIES

##############################

material TAUN=1e-7   TAUP=1e-7   COPT=1.5e-10   AUGN=8.3e-32
AUGP=1.8e-31


#Vacuum

material material=Vacuum real.index=3.3  imag.index=0


#GaAs

material material=GaAs   EG300=1.42     PERMITTIVITY=13.1
AFFINITY=4.07

material material=GaAs   MUN=8800  MUP=400

material material=GaAs   NC300=4.7e17   NV300=7e18

material material=GaAs   sopra=Gaas.nk


# InAs

material material=InAs   EG300=0.36     PERMITTIVITY=15
AFFINITY=4.03

material material=InAs   MUN=30000 MUP=240

material material=InAs   NC300=8.7e16   NV300=6.6e18

material material=InAs   sopra=Inas.nk
```

```
# AlInP (=InAsP)

material    material=InAsP    EG300=2.4    PERMITTIVITY=11.7
AFFINITY=4.2

material material=InAsP MUN=2291 MUP=142

material material=InAsP NC300=1.08e20 NV300=1.28e19

#material material=InAsP sopra=Alinp.nk


# InGaP

material    material=InGaP    EG300=1.9    PERMITTIVITY=11.62
AFFINITY=4.16

material material=InGaP MUN=1945 MUP=141

material material=InGaP NC300=1.3e20 NV300=1.28e19

#material material=InGaP sopra=Ingap.nk


#Gold
material material=Gold real.index=1.2 imag.index=1.8


###############################
#MODELS
###############################
models k.p fermi incomplete consrh auger optr print
models name=well k.p chuang spontaneous lorentz
```

```
###############################
#LIGHT BEAMS
###############################
beam    num=1       am0       wavel.start=0.21      wavel.end=4
wavel.num=50


###############################
#SOLVING I-V CURVE
###############################
log outfile=GaAs_QWs.log
solve init
method gummel  maxtraps=10  itlimit=25
solve B1=1.0
solve vanode=0.0    name=anode      vstep=0.01      vfinal=1


extract name="IV"  curve(v."anode," i."cathode")
extract init infile="GaAs_QWs.log"
extract name="Jsc" y.val from curve(v."anode," i."cathode")
where x.val=0.0
extract name="Voc" x.val from curve(v."anode," i."cathode")
where y.val=0.0
extract    name="Power"    curve(v."anode,"    (v."anode"    *
i."cathode")) outf="Power.dat"
extract    name="Pmax"    max(curve(v."anode,"    (v."anode"    *
i."cathode")))
```

```
extract       name="Vmax"    x.val       from     curve(v."anode,"
(v."anode"*i."cathode") ) where y.val=$"Pmax"

extract name="Jmax" $"Pmax"/$"Vmax"

extract name="FF" $"Pmax"/($"Jsc"*$"Voc")

extract name="Eff" $Pmax/0.1353




##############################
#OUTPUT
##############################
tonyplot GaAs_QWs.log
```

THIS PAGE INTENTIONALLY LEFT BLANK

APPENDIX B. ATLAS SOURCE CODE II

```
#LT EVANGELOS KOLETSIOS HN  *****DEC 2012*****

#This model is a novel Multi Quantum Well GaAs/InAs solar
cell using ORIGINAL parameters with dopant for increased
power.

go atlas
#Definition of constants
#Mesh
#X-Mesh
#Y-Mesh
#Regions
#Electrodes
#Doping
#Material Properties
#Models
#Light Beams
#Solving

#Meshing
mesh width=200000
#mesh space.mult=1
#X-mesh:  Surface=500 um2 = 1/200000 cm2
x.mesh loc=-250 spac=50
x.mesh loc=0    spac=10
x.mesh loc=250  spac=50
#Y-Mesh
#Vacuum
y.mesh loc=-0.1 spac=.01
#Emitter
y.mesh loc=0.000    spac=0.01
#iGaAs
y.mesh loc=0.500    spac=0.05
#wells
y.mesh loc=1.000    spac=0.001
#Base
y.mesh loc=300.000    spac=30


#Regions
```

```
#Vacuum
region num=1 material=Vacuum  x.min=-250     x.max=-50
     y.min=-0.25    y.max=-0.15
#Contact
region num=2 material=Gold        x.min=-50 x.max=50
     y.min=-0.25    y.max=-0.15
#Vacuum
region num=3 material=Vacuum  x.min=50  x.max=250 y.min=-
0.25 y.max=-0.15
#Window
region num=4 material=InAsP   x.min=-250     x.max=250
     y.min=-0.15    y.max=-0.10
#Emitter
region num=5 material=GaAs   x.min=-250   x.max=250   y.min=-
0.10  y.max=0.000
#iGaAs
region   num=6   material=GaAs      x.min=-250      x.max=250
y.min=0.000  y.max=0.500

#Well
region   num=7   material=InAs      x.min=-250      x.max=250
y.min=0.500  y.max=0.505 name=well
region   num=8   material=GaAs      x.min=-250      x.max=250
y.min=0.505  y.max=0.510
region   num=9   material=InAs      x.min=-250      x.max=250
y.min=0.510  y.max=0.515 name=well
region   num=10   material=GaAs      x.min=-250      x.max=250
y.min=0.515  y.max=0.520
region   num=11   material=InAs      x.min=-250      x.max=250
y.min=0.520  y.max=0.525 name=well
region   num=12   material=GaAs      x.min=-250      x.max=250
y.min=0.525  y.max=0.530
region   num=13   material=InAs      x.min=-250      x.max=250
y.min=0.530  y.max=0.535 name=well
region   num=14   material=GaAs      x.min=-250      x.max=250
y.min=0.535  y.max=0.540
region   num=15   material=InAs      x.min=-250      x.max=250
y.min=0.540  y.max=0.545 name=well
region   num=16   material=GaAs      x.min=-250      x.max=250
y.min=0.545  y.max=0.550
region   num=17   material=InAs      x.min=-250      x.max=250
y.min=0.550  y.max=0.555 name=well
region   num=18   material=GaAs      x.min=-250      x.max=250
y.min=0.555  y.max=0.560
```

```
region   num=19   material=InAs      x.min=-250      x.max=250
y.min=0.560  y.max=0.565 name=well
region   num=20   material=GaAs      x.min=-250      x.max=250
y.min=0.565  y.max=0.570
region   num=21   material=InAs      x.min=-250      x.max=250
y.min=0.570  y.max=0.575 name=well
region   num=22   material=GaAs      x.min=-250      x.max=250
y.min=0.575  y.max=0.580
region   num=23   material=InAs      x.min=-250      x.max=250
y.min=0.580  y.max=0.585 name=well
region   num=24   material=InAs      x.min=-250      x.max=250
y.min=0.585  y.max=0.590
region   num=25   material=GaAs      x.min=-250      x.max=250
y.min=0.590  y.max=0.595 name=well
region   num=26   material=InAs      x.min=-250      x.max=250
y.min=0.595  y.max=0.600
region   num=27   material=GaAs      x.min=-250      x.max=250
y.min=0.600  y.max=0.605 name=well
region   num=28   material=InAs      x.min=-250      x.max=250
y.min=0.605  y.max=0.610
region   num=29   material=GaAs      x.min=-250      x.max=250
y.min=0.610  y.max=0.615 name=well
region   num=30   material=InAs      x.min=-250      x.max=250
y.min=0.615  y.max=0.620
region   num=31   material=GaAs      x.min=-250      x.max=250
y.min=0.620  y.max=0.625 name=well
region   num=32   material=InAs      x.min=-250      x.max=250
y.min=0.625  y.max=0.630
region   num=33   material=GaAs      x.min=-250      x.max=250
y.min=0.630  y.max=0.635 name=well
region   num=34   material=InAs      x.min=-250      x.max=250
y.min=0.635  y.max=0.640
region   num=35   material=GaAs      x.min=-250      x.max=250
y.min=0.640  y.max=0.645 name=well
#iGaAs
region   num=36   material=GaAs      x.min=-250      x.max=250
y.min=0.645  y.max=1.000
#Base
region   num=37   material=GaAs      x.min=-250      x.max=250
y.min=1.000  y.max=300

#Electrodes
electrode name=cathode top
electrode name=anode  bottom
```

```
#Doping
doping uniform region=4  n.type    conc=1e19
doping uniform region=5  n.type    conc=2e18
doping uniform region=37 p.type    conc=1e18


#Material Properties
material TAUN=1e-7   TAUP=1e-7   COPT=1.5e-10   AUGN=8.3e-32
AUGP=1.8e-31


#Vacuum
material material=Vacuum real.index=3.3  imag.index=0


#GaAs
material  material=GaAs  EG300=1.42        PERMITTIVITY=13.1
AFFINITY=4.07
material material=GaAs   MUN=8800   MUP=400
material material=GaAs   NC300=4.7e17  NV300=7e18
material material=GaAs   sopra=Gaas.nk


# InAs
material    material=InAs    EG300=0.36     PERMITTIVITY=15
AFFINITY=4.03
material material=InAs MUN=30000 MUP=240
material material=InAs NC300=8.7e16 NV300=6.6e18
material material=InAs sopra=Inas.nk


# AlInP (=InAsP)
material    material=InAsP    EG300=2.4     PERMITTIVITY=11.7
AFFINITY=4.2
material material=InAsP MUN=2291 MUP=142
material material=InAsP NC300=1.08e20 NV300=1.28e19
#material material=InAsP sopra=Alinp.nk


# InGaP
material    material=InGaP    EG300=1.9    PERMITTIVITY=11.62
AFFINITY=4.16
material material=InGaP MUN=1945 MUP=141
material material=InGaP NC300=1.3e20 NV300=1.28e19
#material material=InGaP sopra=Ingap.nk


#Gold
material material=Gold real.index=1.2 imag.index=1.8


models k.p fermi incomplete consrh auger optr print
```

```
#Light Beams
beam    num=1       am1.5       wavel.start=0.21       wavel.end=4
wavel.num=50


#Solving
log outfile=GaAs_InAs_MQWs.log
solve init
method gummel  maxtraps=10  itlimit=25
solve B1=1.0
#solve vanode=0  name=anode  vstep=0.1  vfinal=0.5
solve vanode=0  name=anode  vstep=0.01  vfinal=1

extract name="IV"  curve(v."anode," i."cathode")
extract init infile="GaAs.log"
extract name="Jsc" y.val from curve(v."anode," i."cathode")
where x.val=0.0
extract name="Voc" x.val from curve(v."anode," i."cathode")
where y.val=0.0
extract    name="Power"    curve(v."anode,"    (v."anode"    *
i."cathode")) outf="Power.dat"
extract    name="Pmax"    max(curve(v."anode,"    (v."anode"    *
i."cathode")))
extract      name="Vmax"     x.val     from     curve(v."anode,"
(v."anode"*i."cathode") ) where y.val=$"Pmax"
extract name="Jmax" $"Pmax"/$"Vmax"
extract name="FF" $"Pmax"/($"Jsc"*$"Voc")
extract name="Eff" $Pmax/0.100

tonyplot GaAs_InAs_MQWs.log
```

THIS PAGE INTENTIONALLY LEFT BLANK

APPENDIX C. HELLENIC ALPHABET

Letter	Pronounciation	Uppercase	Lowercase
Alpha	'alpha	A	α
Beta	'veeta	B	β
Gamma	'ŷama	Γ	γ
Delta	'đelta	Δ	δ
Epsilon	'epsilon	E	ε
Zeta	'zeeta	Z	ζ
Eta	'eeta	H	η
Theta	'theeta	Θ	θ
Iota	'ŷota	I	ι
Kappa	'kapa	K	κ
Lambda	'lamđa	Λ	λ
Mu	mee	M	μ
Nu	nee	N	ν
Xi	ksee	Ξ	ξ
Omicron	'omikron	O	o
Pi	pee	Π	π
Rho	rho	P	ρ
Sigma	'siŷma	Σ	σ
Tau	taf	T	τ
Upsilon	'ipseelon	Y	υ
Phi	fee	Φ	φ
Chi	hee	X	χ
Psi	psee	Ψ	ψ
Omega	om'eŷa	Ω	ω

THIS PAGE INTENTIONALLY LEFT BLANK

APPENDIX D. SYMBOLS

Symbol	Description	Unit
a	Angle	deg
α	Absorption coefficient	m^{-1}
α	Lattice constant	Å
AUGN/AUGP	Electron/hole Auger coefficients	cm^6/s
C	Capacitance	F
c	Speed of light	m/s
COPT	Radiative recombination rate	cm^3/s
E	Energy	eV
ε	Dielectric function	–
$\varepsilon_1, \varepsilon_2, n, k$	Optical constants	–
ε_S	Permittivity	F/cm
E_C	Bottom of conduction band	eV
E_F	Fermi energy level	eV
E_g	Energy bandgap	eV
E_V	Top of valence band	eV
f	Frequency	Hz
f(E)	Fermi–Dirac distribution function	–
h	Plank's constant	J·s
$h\nu$	Photon energy	eV
I	Current	A
I_D/I_S	Diffusion/drift current	A
I_{SC}	Short circuit current	A
k	Boltzmann's constant	J/K
kT	Thermal energy	eV

m^*	Effective mass	m_e
μ_n (MUN)/μ_p (MUP)	Electron/hole mobility	$cm^2/V\cdot s$
n	Power conversion efficiency	–
ν	Photon frequency	Hz
N_C/N_V	Electron/hole density of states	cm^{-3}
N_D/N_A	Donor/acceptor impurity atom concentration	cm^{-3}
n_i^2	Majority · minority carrier concentration product	cm^{-3}
n_{n0}/p_{p0}	Majority carrier (electrons/holes) concentration	cm^{-3}
n_{p0}/p_{n0}	Minority carrier (electrons/holes) concentration	cm^{-3}
n_r/n_r^*	Refraction/complex refraction index	–
P	Power	W
1. R	Reflectivity	–
ρ	Resistivity	$\Omega\cdot m$
σ	Conductivity	S/m
T	Absolute temperature	^oK
TAUN/TAUP	Electron/hole lifetimes	s
V	Voltage	V
V_{OC}	Open circuit current	V
χ	Absorption index	–
χ	Affinity	eV

LIST OF REFERENCES

[1]   P. Michalopoulos, "*A novel approach for the development and optimization of state-of-the-art photovoltaic devices using Silvaco,*" M.S. thesis, Naval Postgraduate School, Monterey, California, March 2002.

[2]   S. T. Thornton, *Modern Physics*, Third Edition.

[3]   S.O. Kasap, *Electronic Materials and Devices*, Third Edition.

[4]   Definition of Density of States, Wikipedia, "*Density of states,*" http://en.wikipedia.org/wiki/Density_of_states.

[5]   Atlas Silvaco, *Atlas User's Manual International*, Vol. 1–2, 2007.

[6]   P. Harrison, *Quantum Wells, Wires and Dots*, Second Edition.

[7]   D. J. Griffiths, *Introduction to Quantum Mechanics*, Second Edition.

[8]   A. Luque and S. Hegedus, *Handbook of Photovoltaic Science and Engineering*, 2003.

[9]   M. H. Tsutagawa, "*Triple junction Ingap/Gaas/Ge solar cell optimization using Silvaco Atlas*," M.S. thesis, Naval Postgraduate School, Monterey, California, December 2008.

[10]   S. I. Molina, "Aberration-Corrected Scanning Transmission Electron Microscopy Of Nanostructures For Photovoltaics," *Photovoltaic Specialists Conference (PVSC), 2011 37th IEEE*, pp. 3360–3365, June 2011.

[11]   J. Brübach, "*Ultrathin InAs/GaAs Quantum Wells:Electronic Structure, Excitonic Effects and Carrier Capture*," 2001.

[12]   T. Yoshida, A. Okamoto, S. Muramatsu, N. Kuze, I. Shibasaki, "Magnetoresistance effect of InAs deep quantum well structures grown on GaAs substrates by molecular beam Epitaxy," *Solid State Sensors and Actuators, International Conference IEEE,* Vol 1, pp. 417–418, Chicago 1997.

[13]   "Optimizing Quantum Wells," class notes, Department of Electrical Engineering, Massachusetts Institute of Technology.

[14]   D. B. Jackrel, "*InGaAs And GaInNAs(Sb) 1064 Nm Photodetectors And Solar Cells On Gaas Substrates,*" Doctor of Philosophy, Stanford University, December 2005.

[15]   I. Tomonori, J. Hidenori, A. Toru, N. Kohji, K. Kiyoshi, "An empirical potential approach to the formation of InAs stacking-fault tetrahedron in InAs/GaAs(111)'', *Optoelectronic and Microelectronic Materials and Devices, COMMAD 2008. Conference IEEE,* pp. 86–89, 2008.

THIS PAGE INTENTIONALLY LEFT BLANK

INITIAL DISTRIBUTION LIST

1. Defense Technical Information Center
    Ft. Belvoir, VA

2. Dudley Knox Library
    Naval Postgraduate School
    Monterey, CA

3. Chairman, Department of Physics
    Naval Postgraduate School
    Monterey, CA

4. Dr. Sherif Michael
    Department of Electrical and Computer Engineering
    Naval Postgraduate School
    Monterey, CA

5. Dr. Gamani Karunasiri
    Department of Physics
    Naval Postgraduate School
    Monterey, CA

6. Embassy of Greece, Naval Attaché
    Washington, DC

7. LT Evangelos Koletsios H.N.
    Athens, Greece

9. Hellenic National Academic Recognition and Information Center
    Athens, Greece